Final Technical Report
ONR Grant No. N00014-89-J-1238

A Study of Gas Phase Chemistry of Solid Propellant Ingredients Using a CO_2 Laser

Thomas A. Litzinger
Department of Mechanical Engineering
The Pennsylvania State University

College of Engineering
Department of Mechanical Engineering
University Park, Pennsylvania

Final Technical Report
ONR Grant No. N00014-89-J-1238

A Study of Gas Phase Chemistry of Solid Propellant Ingredients Using a CO_2 Laser

Thomas A. Litzinger
Department of Mechanical Engineering
The Pennsylvania State University

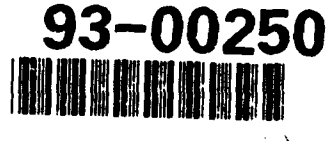

TABLE OF CONTENTS

TABLE OF CONTENTS 1
SUMMARY 2
INTRODUCTION 4
EXPERIMENTAL APPROACH 5
Overall Experimental Facility 5
Experimental Measurement Systems 9
Microprobe/Mass Spectrometer (MPMS) System 11
Mass Spectrometer Unit (MSU) and Related Hardware 11
MPMS Control, Data Acquisition, and Data Reduction 13
Quartz Microprobes 17
Calibration Methods 19
EXPERIMENTAL RESULTS 22
ADN 22
RDX 31
XM-39 Composite Propellant 34
REFERENCES 40

SUMMARY

This research program was designed to address the critical need for data on the gas-phase chemistry of solid propellants through the development and application of a microprobe mass spectrometer (MPMS) system. The MPMS system was used to study the gas-phase chemical reactions occurring above solid propellant ingredients and actual solid propellants when they are heated and/or ignited by the heat flux from a CO_2 laser. In addition to the MPMS system, direct and Schlieren photography were used to study the flame structure and twenty-five micron thermocouples were used to measure the gas-phase temperature profile. During the course of this research program, the majority of tests were performed with ammonium dinitramide (ADN), RDX, and an RDX based solid propellant, XM-39. In addition, preliminary studies of two fuel binders, HTPB and BAMO/NMMO, were performed. This report summarizes the experimental apparatus and the major findings for the oxidizers, ADN and RDX, and the solid propellant, XM-39.

The MPMS was constructed around an Extrel EX500 quadrupole mass spectrometer system chosen for its high performance and its modular design which permitted the system to be tailored to this specific application. The EX500 system is capable of analyzing gaseous species in the mass range of 1-500 amu with scan speeds up to 2000 amu/sec, resulting in a temporal resolution of 0.5 milliseconds. The spatial resolution of the system is approximately 100 μm for a typical microprobe orifice of 20 μm. All the control hardware and software were developed in-house due to the very short durations of the experiments. Extensive efforts were required for the calibration of the mass spectrometer to allow quantification of species including water.

During the study of ADN the experimental conditions covered pressures from 1 to 3 atmospheres of argon and heat fluxes from 50 to 300 W/cm^2. For these test conditions intermittent luminous flames were observed only at higher pressures and heat fluxes. In the absence of a luminous flame, particles were observed which were later identified as ammonium nitrate. The major gas phase chemical species identified in the absence of a luminous flame were H_2O, N_2O, N_2, NO_2, NH_3, and NO. Without a luminous flame present, the temperature of the gases leaving the surface was approximately 700K. When a luminous flame formed, no particles were observed. Through the flame, NO_2, N_2O and NH_3 were consumed. Possible reaction pathways for the decomposition of ADN and the luminous flame reactions were postulated based upon information currently in the literature.

For RDX the experiments were performed at one atmosphere in argon at heat fluxes from 40 to 700 W/cm^2. In all attempts to obtain gas phase temperature profiles, the thermocouples failed very early due to the high flame temperature of RDX. Thus only the surface temperature was obtained; it was found to be approximately 550K. The gas phase species observed were NO, HCN, H_2CO, H_2O, NO_2, N_2O and CO_2. Molecular weight 28, representing CO and N_2, was also observed but the individual contributions of the two species could not be resolved at the time the tests were performed. (Later experiments with XM-39 were successful in resolving the contributions.) The species profiles indicate that H_2CO and NO_2 react near the surface in the primary zone and then HCN, NO and N_2O react in the secondary zone. The species profiles at a heat flux of 100 W/cm^2 indicate that the primary zone occurs from 200 to 300 μm and that the secondary zone begins at approximately 500 μm.

Experiments with XM-39 were performed from 1 to 3 atmospheres in argon and at heat fluxes from 35 to 300 W/cm^2. The species observed are very similar to those observed for neat RDX; however, the primary reaction zone occurs much farther from the surface than for neat RDX extending to nearly 3 mm from the surface at a pressure of 1 atmosphere and a heat flux of 200 W/cm^2. Under no conditions was a secondary flame established. Testing was performed to establish the effect of pressure and heat flux on the location of the primary reaction zone. As pressure was increased the primary reaction zone moved much closer to the surface of the propellant as expected based upon the observations of other researchers. Also, as the laser heat flux was increased the primary reaction zone moved closer to the surface. Temperature profiles in the gas phase were obtained for this propellant because the binder lowers the flame temperature compared to neat RDX.

INTRODUCTION

This research program was designed to address the critical need for data on the gas-phase chemistry of solid propellants through the development and application of a microprobe mass spectrometer (MPMS) system. The MPMS system was used to study the gas-phase chemical reactions occurring above solid propellant ingredients and actual solid propellants when they are heated and/or ignited by the heat flux from a CO_2 laser. The MPMS system uses quartz microprobes with orifice sizes of twenty microns which result in a spatial resolution of approximately 100 microns. In addition to the MPMS system, direct and Schlieren photography were used to study the flame structure and twenty-five micron thermocouples were used to measure the gas-phase temperature profile.

Significant effort was expended in the early part of this program to develop the MPMS system and its controls. Continual refinements were made to the quartz microprobes to achieve smaller orifice sizes and hence better spatial resolution. In addition, calibration of the mass spectrometer presented great challenges as did the separation of molecules of similar molecular weight but dissimilar structures. Other significant challenges were data acquisition and reduction and the synchronization of the laser, the mass spectrometer and the linear positioner used to control the movement of the sample.

The specific goal of this research was to obtain detailed spatial profiles of the major reacting species above the surface of individual propellant ingredients and actual propellants in order to obtain an improved understanding of the controlling chemical processes and of the interactions of binders and oxidizers in heterogeneous propellants. During the course of this research program, the majority of tests were performed with ammonium dinitramide (ADN), RDX, and an RDX based solid propellant, XM-39. In addition, preliminary studies of two fuel binders, HTPB and BAMO/NMMO, were performed. This report summarizes the experimental apparatus and the major findings for ADN, RDX, and XM-39.

In the first section of this report the overall experimental facility and diagnostics are described. Since the development of the MPMS system was a significant portion of the effort in this program, the MPMS, its control systems and its calibration are described in some detail. Following the discussion of the experimental equipment, results from the experiments with ADN, RDX and XM-39 are presented.

EXPERIMENTAL APPROACH

This section of the report describes the experimental setup that was developed for the study of the laser-induced pyrolysis, ignition, and combustion of energetic materials. The overall experimental setup (not including the microprobe/mass spectrometry system) is illustrated in Figure 1; it is described in the first part of this section. Next, the video systems, the schlieren system and the thermocouple measurement method are discussed. Finally the microprobe/mass spectrometry (MPMS) system and all its related components described.

Overall Experimental Facility

The radiative energy source for this research is a Coherent Super 48 high-power CO_2 laser. The laser is capable of producing 800 watts of power in the continuous wave mode and 3500 watts in the pulsed mode with precise control of the power output and lasing time. A power meter connected internally to one of the lasing tube endpieces is used to set the beam power. A beam combiner at the laser output tube allows a He-Ne laser beam to be combined with the CO_2 laser beam and travel along the same axis to facilitate beam alignment. A series of silicon mirrors direct the beam to the test chamber through several sections of aluminum tubes that confine the laser beam. The mirrors can be cooled with liquid coolant flow through the aluminum mirror retaining blocks if long duration (>2 sec) and relatively high heat flux (>500 W/cm^2) tests are to be conducted.

An aperture/lens combination is used to smooth the inherently nonuniform CO_2 laser beam profile. The laser beam passes through a drilled copper plate one meter above the test sample surface and then through an expanding lens (see Figure 1), both of which are mounted on sliding mounts on a vertical aluminum track directly above the test chamber. The 0.64 mm thick copper plate has a 7 mm aperture in its center that allows only the more uniform center section of the beam to be passed on toward the surface. The zinc selenide lens has a focal length of 24 cm and can be moved up or down on the track to expand the laser beam to the desired area at the sample surface. The aperture/lens combination provides a relatively uniform beam profile that varies about 10-15% across the sample surface. A calorimeter, masked by a copper plate with an aperture the same size as the sample diameter (5 mm or 6.4 mm), is employed to measure the incident heat flux at the sample location.

The test chamber is 25.4 cm tall and 16.5 cm on a side with 1.3 cm thick aluminum walls, resulting in an internal volume of 4460 cm^3. This chamber volume is of sufficient capacity so that neither gas removal through the microprobe nor gas generation by the propellant sample

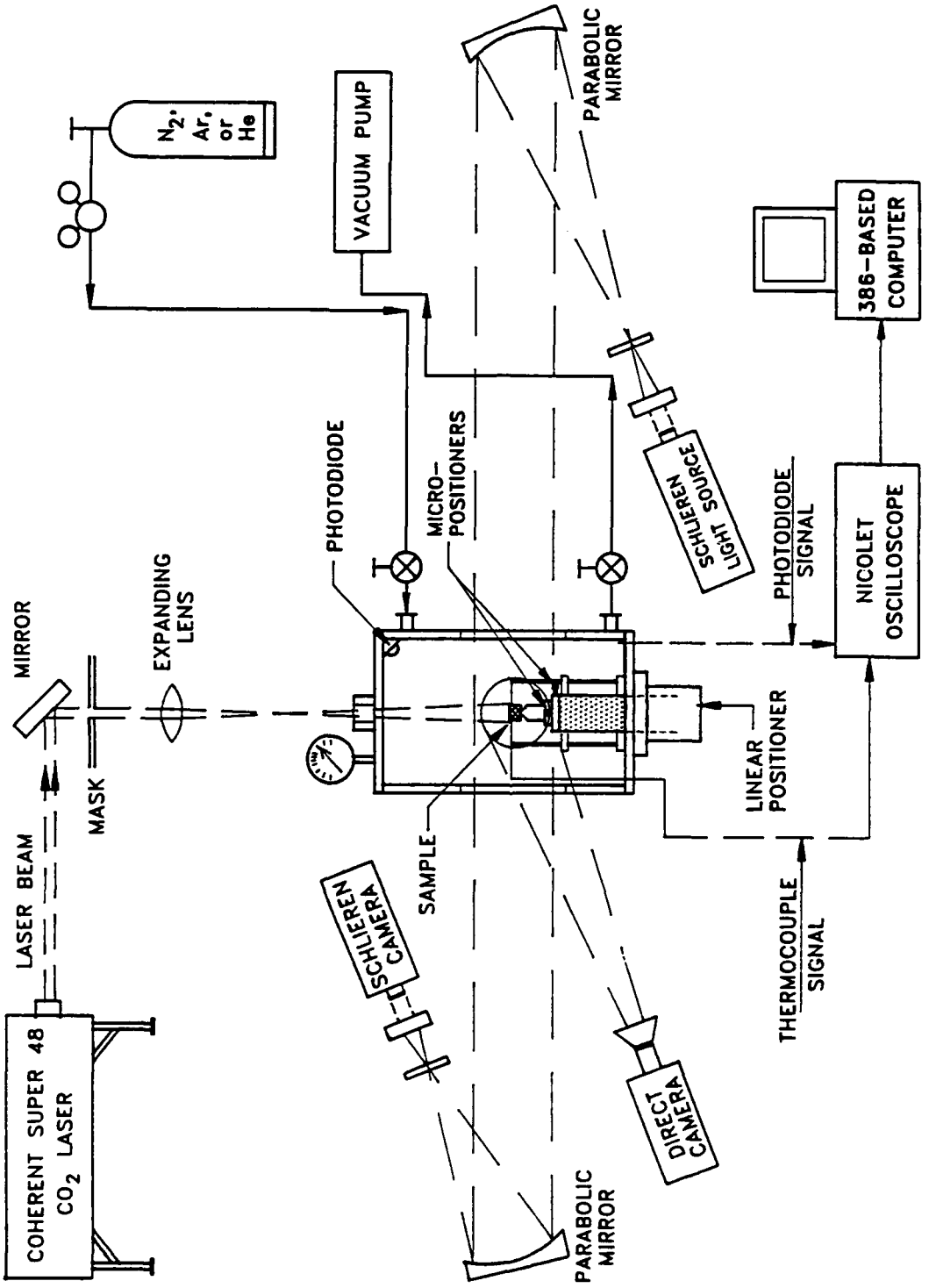

Figure 1. Overall experimental facility for MPMS studies

significantly changes the chamber pressure during the test. All windows in the test chamber are 0.64 cm thick, allowing test chamber pressures above atmospheric to used but not permitting the pressure to be raised above 5 atmospheres. The CO_2 laser beam enters the center top of the chamber through a potassium chloride (KCl) window; an ideal KCl window is 97% transmissive to the 10.6 μm wavelength of the CO_2 laser beam. Two high-quality glass windows are installed in opposite sides of the chamber to allow for passage of the parallel light beam of the schlieren flow visualization system. Another glass window is installed inside the other chamber wall on a spacer plate that positions this window within 3.2 cm of the sample. This windowed test chamber insert allows high-magnification video images to be recorded. An aluminum sealing plate attached to the primary chamber of the MPMS system fits into a machined step in the fourth side of the test chamber. The positioning shaft of a linear positioner enters the center bottom of the test chamber through a hole slightly larger than the shaft. A special synthetic rubber boot O-ring sealed to the chamber permits vertical movement of the positioner and still maintains the chamber pressure and enviroment. All the windows and the primary chamber attachment plate are sealed to the chamber by synthetic rubber O-rings. Several fittings and electrical feedthroughs installed in the chamber walls allow control of the pressure and gaseous environment and sealed passage of the photodiode and thermocouple signals out of the chamber. A rotary vane vacuum pump is used to evacuate the chamber.

The linear positioner and positioner control unit permit precise vertical positioning and movement of the test sample with respect to the position of the probe sampling orifice and the thermocouple bead. The microstepped motor reso-lution of the drive unit is 12,800 steps per revolution which produces a spatial resolution of about 12 μm/step. The shaft acceleration and velocity are variable over a wide range and are computer controlled.

Two different sample holder configurations have been used in this study. In the simpler setup illustrated in Figure 1, the material sample is glued to the sample holder which is attached to two small micropositioners that permit precise X-Y positioning of the sample with respect to the microprobe, thermocouple, and incident laser beam. This whole unit is mounted on top of the linear positioner. This configuration is required for simultaneous direct and schlieren photography and also is the easiest setup for thermocouple tests.

A drawback of the first setup described above is that it does not allow gaseous species sampling along an axis normal to the sample surface. To perform axial sampling, the sample holder configuration illustrated in Figure 2 is used. Both the microprobe and sample surface

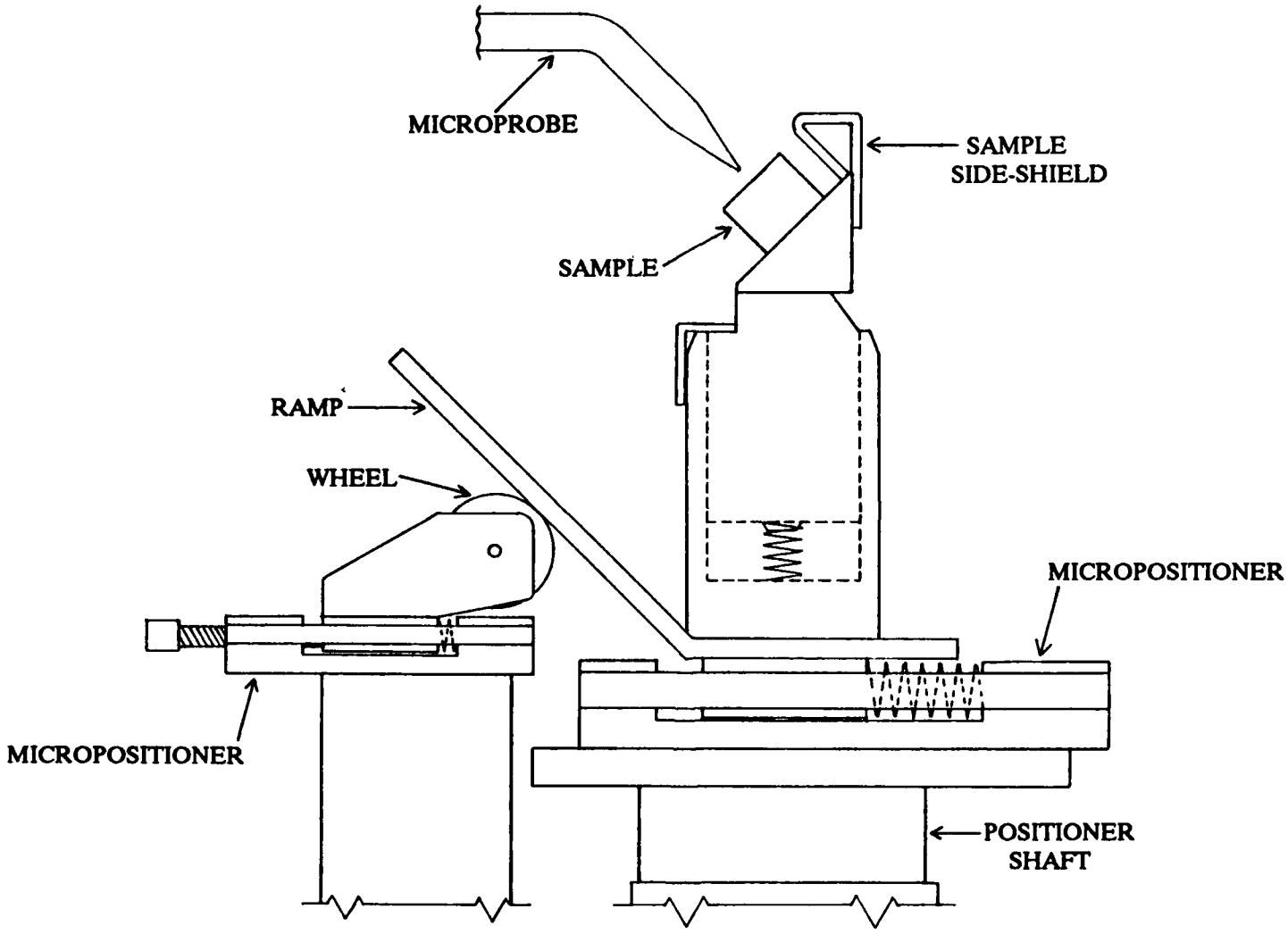

Figure 2. Sample holder for axial sampling

are angled at 45 degree so that they are normal to each other and the laser beam can still irradiate the sample surface. This configuration was also employed by Isom et al. [1]. But to continuously sample along an axis normal to the surface, the sample holder system must move at a 45 degree angle. This is accomplished by mounting a 45 degree ramp under the sample holder and having the ramp ride on a small wheel as the positioner moves upward. The spring in the micropositioner under the holder keeps the ramp in contact with the wheel. The sample holder is spring-loaded by a weak spring and retained inside the outer guide tube by a small sheet metal tab. Spring-loading allows the sample to be driven up to and into the sampling probe without fear of breaking the probe, making it quite safe and easy to obtain profiles right down to the sample surface.

Experimental Measurement Systems

The diagnostic systems illustrated in Figure 1 are discussed in this section. High-magnification video photography is employed to record both direct images of the flame structure and schlieren images of the gas-phase dynamics. Temperature profiles are measured with fine-wire thermocouples. Near-infrared emission is measured with an near-IR photodiode. The related data acquisition and data processing equipment will also be briefly discussed.

Both direct and schlieren images of the laser heating event can be recorded either with a Spin Physics 2000 high-speed video recording system or a SONY CCD V-9 camcorder. The Spin Physics system has a maximum recording speed of 12,000 pictures per second (pps) but produces only a black-and-white image. The SONY camcorder records in color but only at 30 pps. A 5x power magnification lens was fitted to the camcorder and, when used in macromode in the windowed test chamber insert, the magnified image seen on the TV monitor is 16-20 times the actual size. This provides good spatial resolution for accurately determining sampling heights. A strobe light that is actuated coincident with the laser trigger signal marks zero-time on the video movies by generating a single-pulse flash recorded by the camera.

The schlieren system is oriented in a Z-type configuration. The source light produced by a 100 watt continuous tungsten-halogen lamp passes through a condensing lens and then through a rectangular aperture with four movable knife-edges that allow precise control of the slit geometry. The beam is then collimated into a parallel beam by a parabolic mirror placed a focal length away from the knife-edge. The beam passes through the chamber windows and is then reflected by an identical parabolic mirror through another adjustable rectangular aperture. This

aperture permits control of the amount of deflected light blocked by the knife-edges which determines the schlieren system's sensitivity. The light beam then passes through a collimating lens directly into the Spin Physics camera or is directed onto a frosted glass screen from which the camcorder records the image.

A near-infrared photodiode is employed to monitor visible/near-IR emission from the sample surface or the gas-phase directly above the surface. The spectral response of the photodiode is from 0.35-1.10 μm with peak sensitivity at 0.9 μm. The photodiode is mounted on a bracket attached to the primary chamber flange and is located 11 cm above the sample surface and 2 cm from the laser beam centerline with the photodiode's optical axis aimed at the sample surface. The emission profiles can be used to determine ignition delay times where ignition is defined as the point at which the first abrupt and sustained increase in the emission output occurs. The emission profile under laser-augmented combustion can also be used as an indicator of the combustion stability.

Fine-wire thermocouples are used to measure sample surface temperatures and to obtain gas-phase temperature profiles above the sample surface. Both chromel-alumel and platinum-platinum/13% rhodium thermocouples with wire diam-eters of 25 and 50 μm have been purchased from Omega Engineering, Inc. However, these prefabricated thermocouples have bead diameters that are sometimes as much as 3-5 times the diameter of the wire, which greatly reduces both the spatial and temporal resolution of the measurement. When resolution is critical, this problem is avoided by precisely welding 25 μm diameter platinum and platinum/13% rhodium wires together under a microscope to obtain the smallest bead possible. With a little practice, it is relatively easy to obtain junction sizes the same size as the wire diameter or slightly smaller, resulting in very fast response times of two milliseconds or less. A thermocouple stand supports the thermocouples over the sample and allows for height adjustment (see Figure 1). Two brass tubes fastened to an aluminum plate contain the thermocouple extension wires to which the thermocouple wires are soldered.

A Nicolet 310 digital oscilloscope is used to record both the photodiode and thermocouple signals. The thermocouple signals are amplified by a wideband preamplifier before being recorded on the oscilloscope. The scope operates at a maximum recording speed of 1 Mhz and has two input channels. The system records the data on 3.5" disks in DOS-compatible format so that they can be read directly by a PC-compatible computer. VU-POINT software is used to process the data. The oscilloscope is triggered by a signal output from the CO_2 laser at the point of laser trigger that signals the zero-time for the test.

Microprobe/Mass Spectrometer (MPMS) System

This section is divided into several subsections beginning with a description of the mass spectrometer unit (MSU) and the mass spectrometer electronic control system. The computer control, data acquisition, and data reduction operations are then discussed, followed by a discussion of the quartz microprobes used for gas species sampling. The last subsection presents the calibration methods used.

The hardware constituting the MPMS system is illustrated in Figure 3. An Extrel EX500 quadrupole mass spectrometer system was chosen because of its high performance and its modular concept which permitted much flexibilty in the choice of components to tailor the system to this application. The EX500 system is capable of analyzing gaseous species in the mass range of 1-500 amu with a scan speed variable between 0.2 and 1000 amu/sec. A resolution of 3000 is obtainable at a mass of 500 amu, and the sensitivity is 4 ma/torr at mass 28 amu before electronic amplification.

Mass Spectrometer Unit (MSU) and Related Hardware

The Extrel mass spectrometer unit depicted in Figure 3 performs the ionization, mass filtering, and detection of the sample gaseous species. The gaseous species are drawn into the MPMS sytem by two pumping stages and pass through two microprobe orifices, forming a beam of gaseous species. This beam enters the unit through an axial ionizer. Ions produced by the ionizer are then directed into the quadrupole mass filter by an extractor, three focusing lenses, and an ELFS unit that counteracts the detrimental fringe field effects of the mass filter. The quadrupole mass filter electromagnetically filters out the ions of the desired mass to charge (m/e) ratio and allows them to pass on through an exit focusing lens to the detection system that consists of a conversion dynode (CD) combined with a Channeltron multiplier. The multiplier output signal then passes through a preamp and is either displayed on a monitor or recorded and processed with a computer.

A two-stage pumping system is employed to obtain the required low pressures for the MPMS system (see Figure 3). A mechanical rotary vane pump with a pumping speed of 85 liters/min evacuates the primary chamber. The pump is specially constructed to be able to evacuate corrosive gases without serious degra-dation of the internal pump components. The

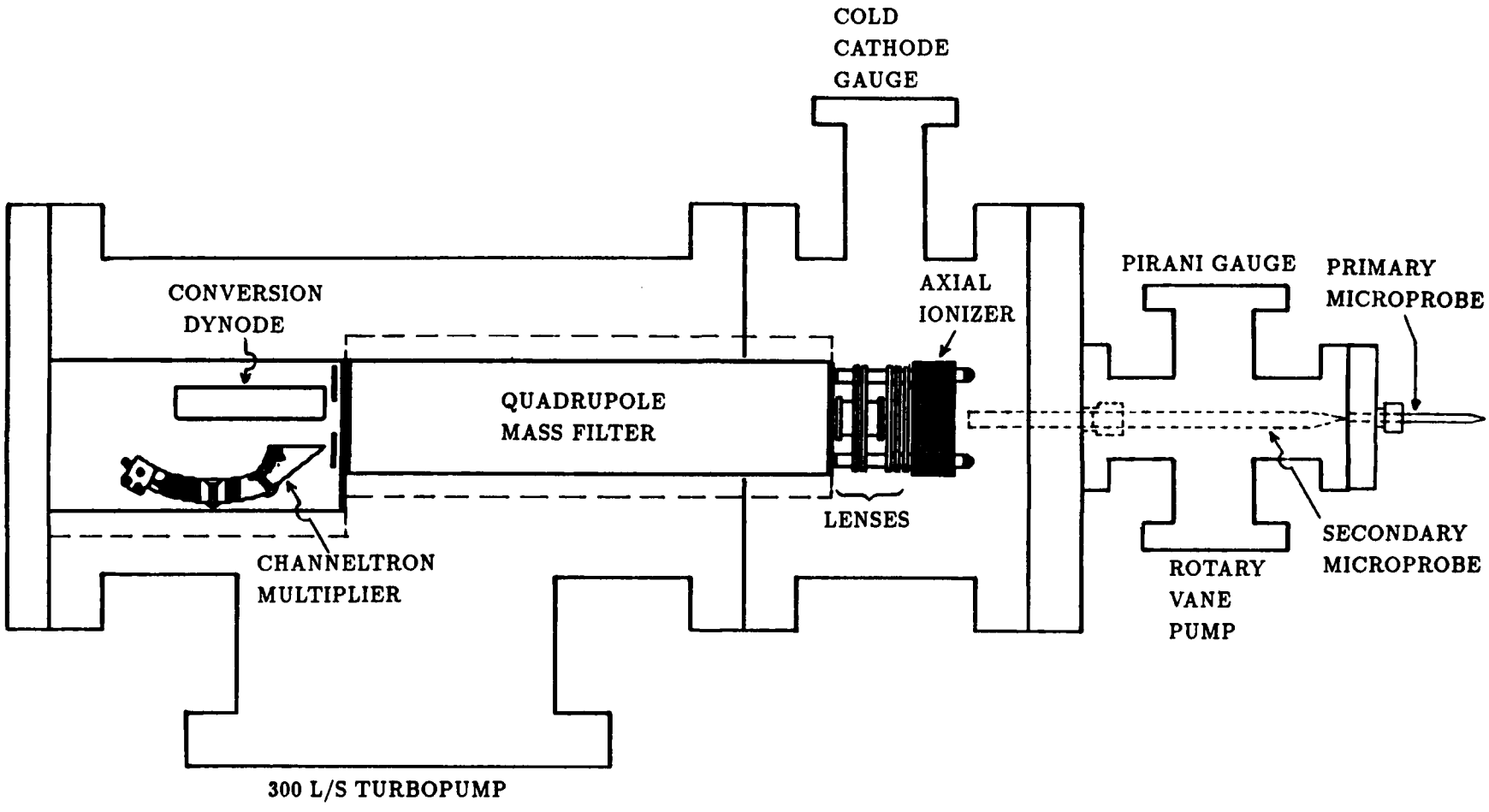

Figure 3. Schematic of MPMS system

quadrupole probe chamber containing the MSU is evacuated by a Balzers turbomolecular pump system capable of a pumping speed of 300 liters/sec. The turbopump is exhausted by a backing pump with a pumping speed of 360 liters/min. Magnetic floating bearings provide rotating support for the turbopump rotor and are impervious to the corrosive gases that may be generated by the burning sample. Quartz microprobes are employed as the gas inlets for each stage. The design and construction of these microprobes will be discussed in detail in a later section.

The MPMS system is enclosed in several housings interconnected with Del-Seal flanges and copper gaskets. A Pirani gauge and a cold cathode gauge are employed to measure the pressures in the primary and quadrupole chambers, respectively. The cold cathode gauge is interlocked with the Extrel electronics so that all power to the MSU is immediately shut down if the quadrupole chamber pressure exceeds $1x10^{-4}$ torr. Representative pressures for sampling at one atmosphere by a microprobe with a 25 μm orifice are a primary chamber pressure of 0.2 torr and a quadrupole chamber pressure of $2x10^{-6}$ torr. The back mounting flange for the MSU assembly includes feedthroughs for the RF cables and ionizer cable and five other BNC-type feedthroughs. The flange also has a 3.4 cm sight glass installed on the geometric axis of the MPMS system that provides optical access for precise alignment of the components.

As seen in Figure 3, the MSU is housed in a large "Tee" fastened directly to the top of the turbopump. An additional length of tube was required to accommodate the long high-performance quadrupole rods. A large flange seals the front of this additional tube and contains an axially-aligned 0.64 cm CAJON Ultra-Torr fitting for installation of the secondary microprobe. Attached to the four-way cross that constitutes the primary chamber are a fitting and hose leading to the rotary vane pump, the Pirani vacuum gauge, and a flange that has a 0.32 cm CAJON Ultra-Torr fitting for the primary microprobe. An aluminum sealing plate that fits into an O-ringed step in one of the test chamber walls is installed behind the front flange of the cross to secure the test chamber to the MPMS system.

MPMS Control, Data Acquisition, and Data Reduction

Figure 4 displays the various electronic control units and inter-connections employed in the MPMS system. The Extrel electronic systems that power and control the MSU consist of a DC power supply, a booster power supply for analysis in the higher amu range, a modular mainframe, and a quadrupole control (QC) unit. The components that process and display the

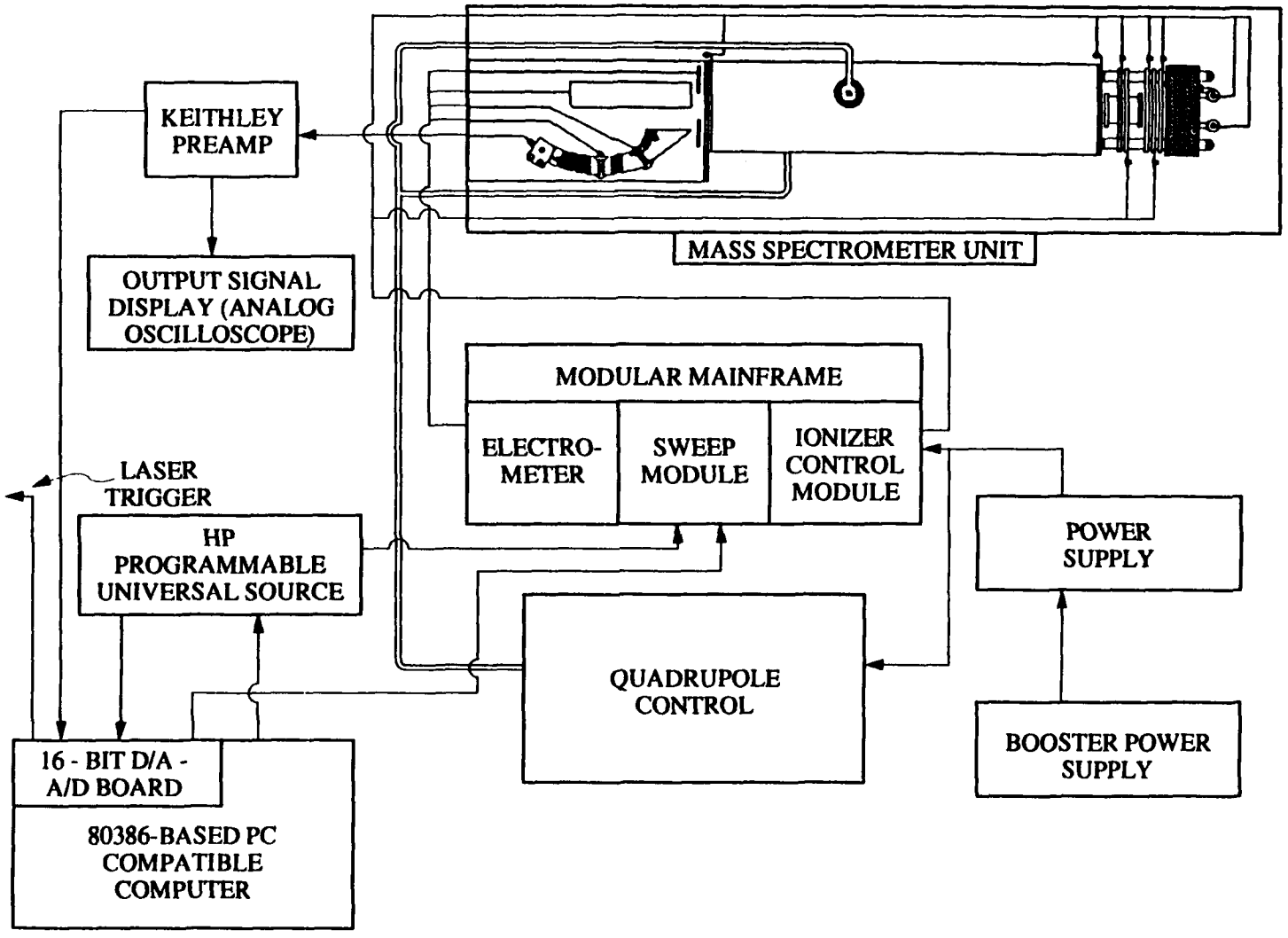

Figure 4. MPMS control electronics

output signal include a preamp, an analog oscilloscope, and a 80386-based PC compatible computer accessed through a high-speed I/O board. A Hewlett Packard universal source (HP-3245A) programmed by the computer is used for control of the mass spectrometer.

The modular mainframe provides for manual or computer control of the system electronics and consists of the ionizer control module, the sweep module, and the electrometer module. The ionizer control permits manual or computer control of the ionization energy from about 10 to 100 eV and electron emission current from 0.1 to 30 milliamps. Emission current is commonly set at 0.2 ma to prolong filament life. The ionization energy is commonly set at various levels from 14 to 22 eV to avoid fragmentation of the parent molecules and to allow for separation of species at the same molecular weight by differences in their appearance potential. The ionizer control also allows for precise regulation of the ion energy, extraction potential, and the focusing lens voltages through a set of potentiometers. The electrometer module permits choice of the mode of detection (usually the CD/multi-plier combination is used) and allows control of the multiplier input voltage, which determines the multiplier gain. The sweep module commands the quadrupole control unit that generates the RF and DC signals to control the operational parameters of the quadrupole mass filter, such as the amu sweep speed and starting mass for the mass scan. During MPMS tests, this module is controlled by the HP-3245A.

The output signal from the multiplier is amplified by a Keithley analog current amplifier. The Keithley preamp replaces the original preamp from Extrel and greatly enhances the electronic speed of the system, improves the signal-to-noise ratio, and allows greater freedom in choosing the optimum gain setting for amplifying the multiplier output signal. The signal generated by the preamp is displayed on a monitor (analog scope) and/or input to the computer through a high-speed I/O board. The real-time experimental control, data acquisition, and data reduction for the MPMS system are all performed through an 80386-33 IBM PC compatible com-puter. The Hewlett Packard programmable universal source (HP-3245A) is used for precise control of the MPMS system and for increased flexibility in selecting the specific amu or amu range to be sampled during the test event. The HP-3245A generates precise DC voltage outputs from -10 to +10 VDC with 6 digits of resolution (24 bits). It can be programmed to generate arbitrary waveforms up to 1 MHz or ramp waveforms up to 100 KHz and can also generate trigger signals.

A Data Translation high-speed D/A-A/D board provides an additional I/O link for the computer to the various systems. The board is capable of a maximum sampling rate of 100 KHz that can be divided among four A/D inputs, has 16-bit output voltage resolution, and permits

simultaneous output of analog signals through two D/A channels. In the current setup depicted in Figure 4, one of the D/A channels triggers the CO_2 Laser while two A/D channels are employed, one to read the output signal from the Keithley preamp and the other to record the MS control signal generated by the HP-3245A.

The control of the MPMS system, data acquisition, and data reduction are all performed through two main computer programs, the mass spectrometer control and data acquisition program (DATACQ) and the data reduction program (DATREDUC). These programs are set up in a windows/multiple menus environment using Turbo Pascal 5.0 as the programming language and the Turbo Technojock's Toolkit for many of the user interface procedures.

The DATACQ program contains several modules chosen through the main menu which permit the user to input the desired test control parameters and actuate the entire system. The Mass Command module allows the user to build, load, edit, save, and graphically display the mass command array. The mass command array can consist of either specific amu values with selected mesurement durations (usually 0.5-1.5 ms) or a series of amu ramps that scan a range of molecular weights at a chosen speed. The array can accept up to 12 individual amu values and is looped continually throughout the desired duration of the test. Initiation of the Begin Run Mode module allows the user to set the initial sample position with the linear positioner. Once the desired position is achieved, the user inputs an array of desired positioner velocities or sample positions and the time durations for each entry. The computer takes this data, interprets it, and programs the positioner prior to the test through a parallel port connection. The positioner is triggered to execute the program by the computer at the beginning of the experimental run. After programming the posi-tioner, the user then proceeds to establish the duration of the data acquisition and name of the file that will contain the data obtained from the mass spectrometer. The program then waits for the user to initiate the test. Upon initiation, the computer triggers the laser, begins the data acquisition process, and sends a signal to the positioner to execute its movement program. When the test is completed, the computer transfers the data to a file and returns to the main menu.

The Data Reduction program (DATREDUC) is a separate program which is used to read and evaluate the data files created by DATACQ. The final output from this program is a file of numbers representing the absolute peak intensities as a function of sampling time for each of the peaks (i.e., amu values) reduced in the reduction analysis. The data file produced by DATACQ is displayed in a graphical window and consists of both the amu control parameters and the raw data from the mass spectrometer as a function of run time. The modules available in

DATREDUC for data processing are the Edit Display, Select Loop, Edit Data Filters, and Reduce Data modules. The Edit Display module allows the scales for the time, amu control signal, and MS output signal to be changed to simplify data processing. The Select Loop module lets the user interactively select the start and end points for a representative mass command array loop which the computer then uses to define the durations for all the loops in the file. Choosing the Edit Data Filters module then gives the user a starting marker and ending marker which can be moved to enclose a small range of data points in each peak. After all the data markers for the peaks of interest are chosen, selecting the Reduce Data module prompts the computer to average the chosen range of data points for each peak in each loop. The result is an output file of absolute species intensities as a function of sampling time. This file is then imported into a spreadsheet program (Microsoft Excel) for final evaluation and graphing.

Quartz Microprobes

The microprobes are fabricated from quartz tubing 2 mm I.D. by 3.2 mm O.D in size for the primary microprobes and 4 mm I.D. by 6.4 mm O.D. for the secondary probes. The probe construction method is fundamentally the same as that detailed by Fristrom and Westenberg [2] except for the method of producing the final probe orifice size. The quartz tubing is placed in a dual-chuck lathe and spun at low rpm while being heated by a small torch over an area roughly equivalent to the length of the desired probe nose. One chuck of the lathe is slowly pulled away, causing the tubing to neck down in a conical geometry to a very small diameter region in the center of the heated area. The inside of the tubing is totally closed off in th' ; region. The tubing is then cut at the narrowest point with a diamond wheel, producing two probes with conical noses. Each probe is cut to length and the conical outside surface of the nose is gently ground with the side of the diamond wheel to obtain the smallest outside diameter possible for the probe tip.

Figure 5 gives a more detailed illustration of the gas sampling setup from the primary microprobe entrance to the ionizer entrance. The CAJON Ultra-Torr fittings are bored through so that the microprobes can be slid through the fittings, allowing flexibility in positioning. The tip of the secondary microprobe is positioned less than 1 mm from the exit of the primary microprobe. Precise alignment of the two probes' axes is attained with a centering fixture installed in the primary chamber tube to support the secondary microprobe. This positioning and alignment of the secondary microprobe enhances its sampling efficiency, improving the signal strength and the signal-to-noise ratio by reducing the amount of

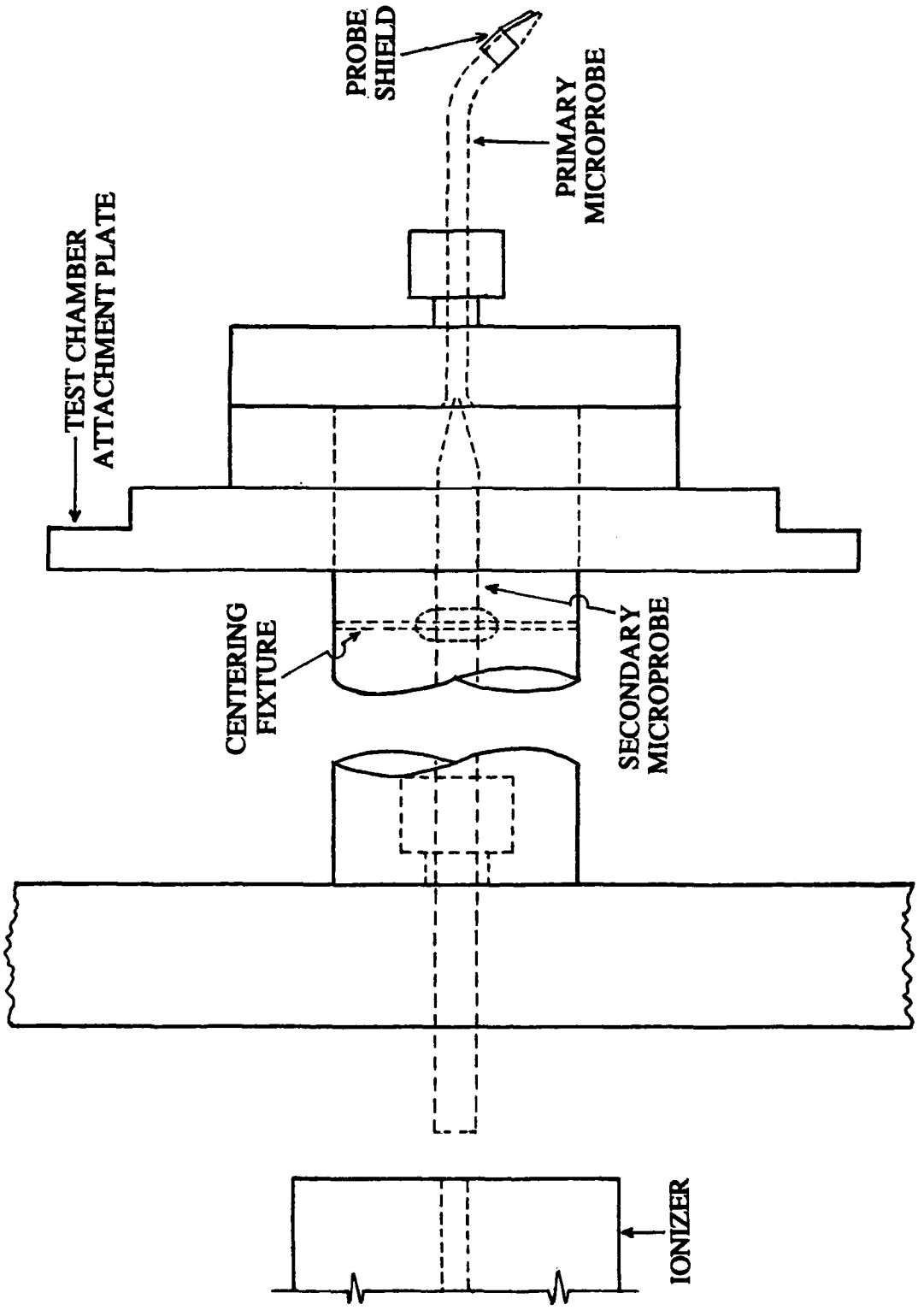

Figure 5. Schematic of gas sampling approach

background gases that can be entrained in the sample gas beam. The exit of the secondary microprobe is about 0.64 cm from the ionizer entrance. Also seen in Figure 5 is a beam shield that protects the primary microprobe from undesirable radiative heating by the incident laser beam. The shield is made of 0.64 mm thick copper sheet, which has a reflec-tivity of about 97% at the laser's wavelength of 10.6 μm.

The method of probe construction allows the probes to be finished to fine dimensions both in external size, reducing the intrusiveness, and in sampling orifice size, which greatly enhances the spatial resolution of the sampling system. The blank probes are finished with manual sanding by first using coarse grit sandpaper to reduce the probe tip dimensions to the desired sizes. Fine grit sandpaper is then used to polish the final external surface and to carefully sand back the face of the probe tip until the desired sampling orifice size is obtained. All operations are carefully monitored under a 12 power illuminated aspheric magnifier. However, even with the magnifier, the desired sampling orifice sizes of 15-25 μm are difficult to see, not only due to the small size but also due to the possibility of sanding grit blocking the hole. To circumvent these difficulties, final sanding of the tip with the 600 grit sandpaper is performed in a small, shallow dish of water with air pressure of about 20 psig applied to the back of the probe through a Tygon tube. As soon as the blank probe tip is sanded through and an orifice develops, tiny air bubbles are observed in the water bath. The air flow keeps the orifice free of debris and the size and frequency of air bubbles is a strong initial indicator of the probe orifice size. The actual orifice size is determined by sizing it with fine-wire thermocouple wires and by experimentally measuring the flow through the microprobe. With this setup, the probes can be carefully and accurately finished to small external dimensions to make the probe as nonintrusive as possible. Tip diameters of 200-250 μm are currently being used and are easily obtained.

Calibration Methods

To determine quantitative gaseous species profiles, the product gaseous species must be calibrated. Calibration is performed by fitting a small calibration chamber over the microprobe and fastening and sealing it to the MPMS primary chamber flange. The chamber is then filled with gas mixtures of known concen-trations which, if possible, are chosen to be close in concentration to the product gas composition expected to be evolved by the deflagrating material. Peak signal intensities I_i in millivolts (mv) are recorded as a function of the ionization potential setting for the ionizer and the species concentration C_i with respect to a given signal standard. The signal standard for most of these tests is a 5 volt signal intensity for pure argon at 22 eV. Sensitivity coefficients $K_{i,j}$ (units of mv/%) are then calculated for each molecular species i and each atomic mass unit (amu) j appearing in the mass spectral pattern at that particular ionization

potential (e.g., the signal standard setting listed above for argon gives $K_{Ar,40}$=50 mv/%). Calibration of stable gaseous species is performed each day a series of tests is to be conducted.

The sensitivity coefficient for water is obtained by filling a small glass cup (dia.=1 cm) with water, placing it on a flat sample holder under the microprobe, filling the chamber with argon, and vaporizing the liquid with the CO_2 laser. Signal intensities for argon and water are then recorded. Since the gas mixture has only these two components and the concentration of argon is easily determined with $K_{Ar,40}$ given above, the concentration of sampled water can be resolved and the sensitivity coefficient $K_{H2O,18}$ can be determined. The sensitivity coefficients for calibrated gaseous species are usually assumed to be constant over the range of concentrations that are experimentally observed. However, the test results for this system indicate that this is a poor assumption for water that may lead to large errors when quantifying the water concentration. Thus, the calculation of the water concentration requires simple iteration using the data. This significant variation in the sensitivity coefficient was not observed with any other gases that have been calibrated.

In order to separate the signals contributed by different species with the nearly the same molecular weight, such as N2 and CO, experiments were performed at different levels of electron energy to eliminate signals from one of the components. When this procedure was applied to N2 and CO quite unreasonable results were obtained when the calibration factors from calibration at room temperature were used. This behavior appears to be related to the internal energy of the molecules at elevated temperature when electron energies are very near the ionization threshold energy. For CO, calibrations were performed during the oxidation of teflon which produces no nitrogen and therefore does not suffer from the interference of nitrogen. Based upon the calibration factors obtained, data from a test with XM-39 were re-reduced and yielded greatly improved atom balances. These results are presented in Figure 6.

To determine the mole fractions of the sampled gases, the resulting concentrations were summed and each concentration was divided by the total. These normalized mole fractions may not exactly represent the true mole fractions if some species are not measured. Therefore, it is important to consider all possible species in a given system to minimize any deviation from true mole fractions. This method of calculating mole fractions cancels out the temperature dependency of the species concentrations and also cancels out the effect of signal reduction by slight probe orifice constriction during a test.

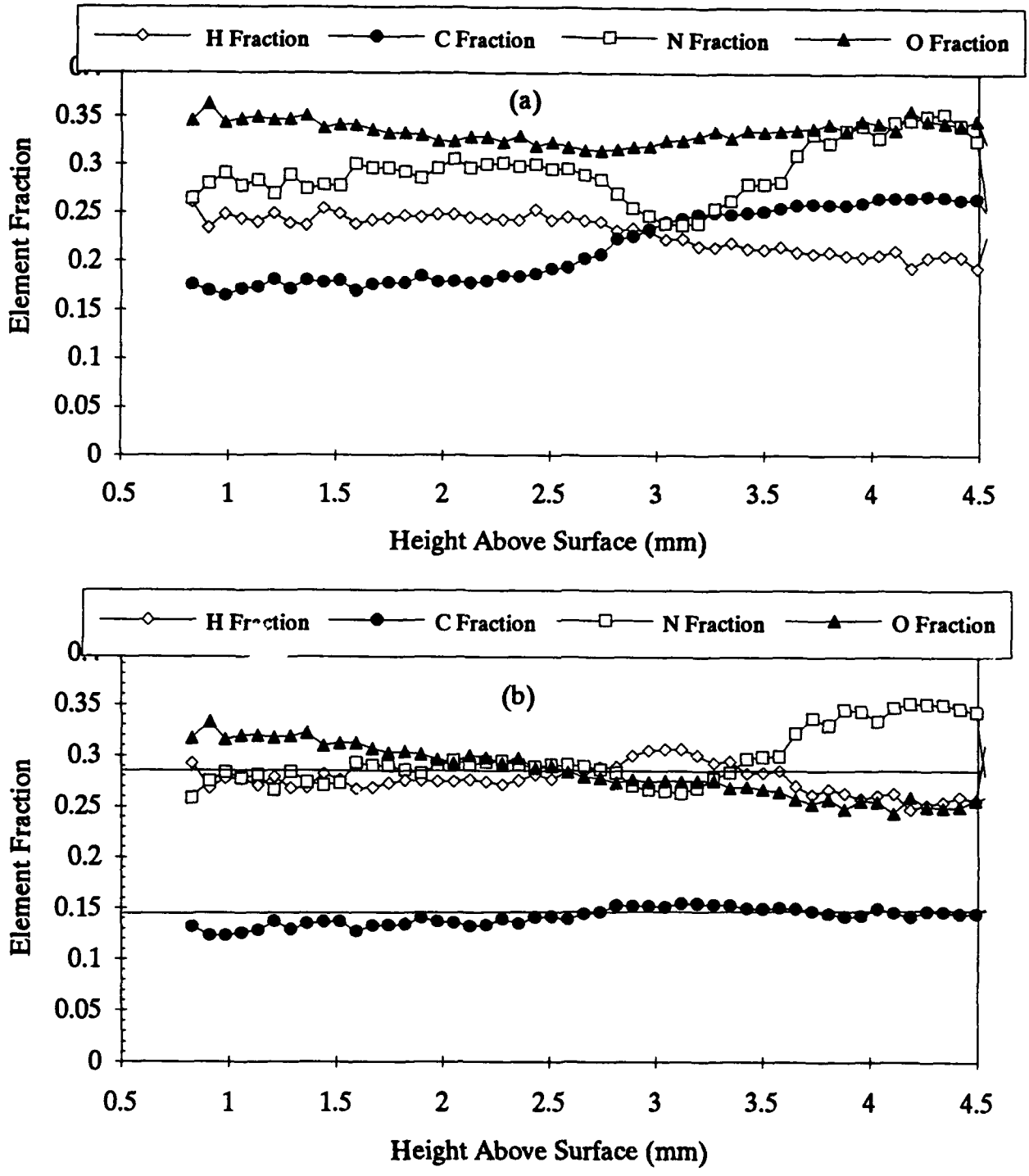

Figure 6. Comparison of atom balance for XM-39 test using early calibration factor of CO (a) to that with most recent calibration for CO at low eV (b).

EXPERIMENTAL RESULTS

This section of the report summarizes the experimental results and presents major findings. The results for the two oxidizers, ADN and RDX, are discussed first and then the results for the heterogeneous propellant,XM-39, are described. For ADN and XM-39 the effects of variation in heat flux and pressure are reported. Important observations made concerning physical processes are also noted.

ADN

At an ambient pressure of one atmosphere of argon, laser heating of the ADN samples with heat fluxes of 50-300 W/cm^2 produced vigorous evolution of gases from the surface and a quite steady regression rate but did not produce a luminous flame. Initially, laser heating of the sample caused a melt layer to develop on the surface. However, after a certain interval of time (on the order of 80 ms for a heat flux of 100 W/cm^2), the onset of vigorous gas evolution was observed for all tests at one atmosphere and the sample surface regressed in a quasi-stable manner. Tiny bubbles in the surface melt layer were observed when recovered samples were inspected under a 12x magnifying lens. For some tests at lower heat fluxes, the height of the melt layer grew significantly during laser heating and then very abruptly dissipated upon the onset of vigorous gas evolution. Coinciding with this abrupt melt layer dissipation was the evolution of a dense cloud of particles, followed by steady particle evolution observed as a smoky plume. The post-test chamber atmosphere was opaque over the chamber inner width of 14 cm due to the optically thick suspension of particles. Since the ratio of the chamber volume to the initial sample volume is around 30,000:1, these observations indicate that the quantity of particles produced by the ADN sample under these test conditions was substantial.

A quasi-steady luminous flame was observed for tests at three atmospheres of pressure. The onset of the flame was observed either coincident with the beginning of rapid gas evolution or occurring shortly thereafter. However, the flame was not very stable and often exhibited random patterns. The flame seemed to be strongest at the edges of the gas plume evolved from the sample surface. This may imply that the lower velocity of the evolved gases in the shear layer between these gases and the ambient argon promotes the stabilization of a flame. The luminous flame appeared to stand off from the surface roughly 0.06 to 0.15 cm. However, thermocouple measurements did not give evidence of a flame zone over the central portion of the sample surface at this height. When the luminous flame was established, few if any particles were observed.

Thermocouple tests were conducted in conjunction with video imaging to investigate both the surface temperature and the temperature profile through the gas phase under laser heating. Figure 7 displays three temperature profiles in the gas-phase up to a height of 0.3 cm above the sample surface at two different pressures and three different heat fluxes. For the test at three atmospheres, the temperature rose to a maximum of about 1250 K at 3 mm above the surface before the sample was consumed. Although temperature profiles including the primary flame were not obtained, approximate flame temperatures of 1250-1330 K were measured in several tests where an erratic flame occurred or the thermocouple passed through the flame zone on the side of the evolved gas plume. An energy balance based upon the post-flame species mole fractions (given below) predicted a temperature of 1275 K which is quite consistent with these observations. The two thermocouple traces for tests at one atmosphere display a relatively constant temperature with a slight rise over the measurement interval. Even though the level of incident heat flux differed by a factor of six for the two tests at one atmosphere, the two traces are quite similar in temperature, indicating that the heat flux level has little effect on the physical and chemical processes occurring in this region. This observation agrees well with the observations of the regression rate made during these tests which showed it to be insensitivite to the incident heat flux. For the test at three atmospheres, the pre-flame temperature was approximately 100 K higher than the temperature in this same zone for tests at one atmosphere.

The surface temperature of the reacting ADN sample was difficult to measure because of the high velocity gases evolved from the surface. These gases would blow the thermocouple bead off the surface before the surface temperature could be measured. A test was conducted to avoid this phenomenon by initially embedding the thermocouple in the melt layer on the surface and then running the test. Embedding thermocouple was accomplished by heating a sample, with a thermocouple bead on the surface, for only 100 milliseconds so that melting occurred but vigorous gas evolution did not. Post-heating analysis of the sample clearly showed that the thermocouple was embedded in the rehardened surface melt layer. Upon further laser heating, the thermocouple trace showed a rapid rise in temperature up to 600 K within 30 ms and then dropped to a relatively constant value of 570-580 K for 25 ms which is believed to be the surface temperature under these conditions. The temperature then rose rapidly to a temperature of 700 K. The precise location of the thermocouple bead during the most rapid rise of the gas-phase temperature could not be resolved from the videos, but the timing of the rise implies that it was just above the surface, suggesting the existence of a near-surface gas-phase reaction zone.

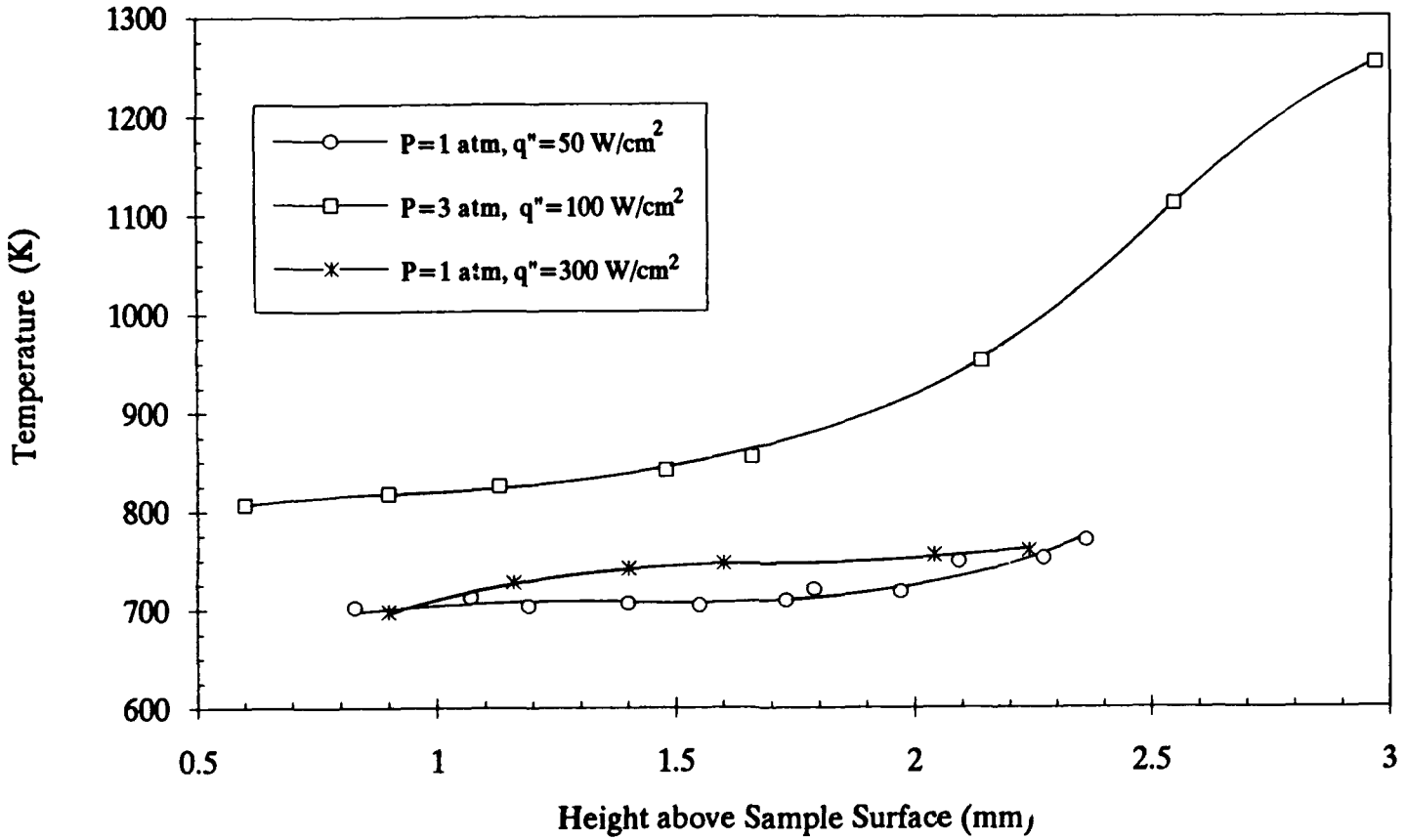

Figure 7. Thermocouple traces for three laser heating tests of ADN

Spatial species profiles for a representative test in one atmosphere of argon are displayed in Figure 8a. The species concentrations were observed to be quite constant in this region under these test conditions. This observation is consistent with the lack of temperature change displayed in Figure 7. Figure 8 indicates species profiles only to within 0.4 mm of the surface due to slight clogging of the microprobe by evolved particles as the probe was moved towards the sample. However, several other tests were conducted where the probe reached the surface without clogging. In those tests, no significant changes in species concentrations and no other detectable species were observed as the probe approached the surface. Additional tests were conducted at sub-atmospheric pressures and at low heat fluxes in an attempt to detect primary species evolved during the pyrolysis of ADN. However, no species other than those shown in Figure 8 were detected.

The results of an atom balance for the data displayed in Figure 8a are given in Figure 8b. Since ADN contains equal numbers of N, H, and O atoms, the total content of each element in the product species should be one-third of the total elemental content of the products. The oxygen content of the detected species was close to 30%, but the nitrogen content was high and the hydrogen content was low. The source of this imbalance was believed to be the condensed-phase particles evolved. These particles were believed to be ammonium nitrate (AN) which Brill et al. [3] detected in their T-jump/FTIR tests of ADN. Analysis of the particles from the MPMS experiments using the Gandolfi method of x-ray diffraction indicated that they were indeed AN. Bringing the measured species concentrations into agreement with the expected atom balance required the inclusion of 0.15 mole fraction of AN. This amount of AN is higher than the 0.05 mole fraction of AN proposed by Brill et al. for high heating rate pyrolysis of ADN, but could be realistic given the different experimental conditions between the two types of experiments.

Species profiles and the accompanying atom balances for a test at three atmospheres in argon and a heat flux of 100 W/cm^2 are displayed in Figure 9. The probe was initially positioned 1.0 cm above the sample surface with no subsequent positioner movement. Initially, the species mole fractions are quite close to those seen in Figure 8a. However, as a flame develops, species production and consumption are evident. O_2 is not depicted in Figure 9a, but a small amount of O_2 was produced by the flame reactions with a peak mole fraction of 0.015 at 250 ms. It is evident from Figure 9a that the transient flame only lasted about 100-150 milliseconds and then dissipated, evidenced by the return of the species mole fractions to those observed at the beginning of the graph. The video images showed that a substantial

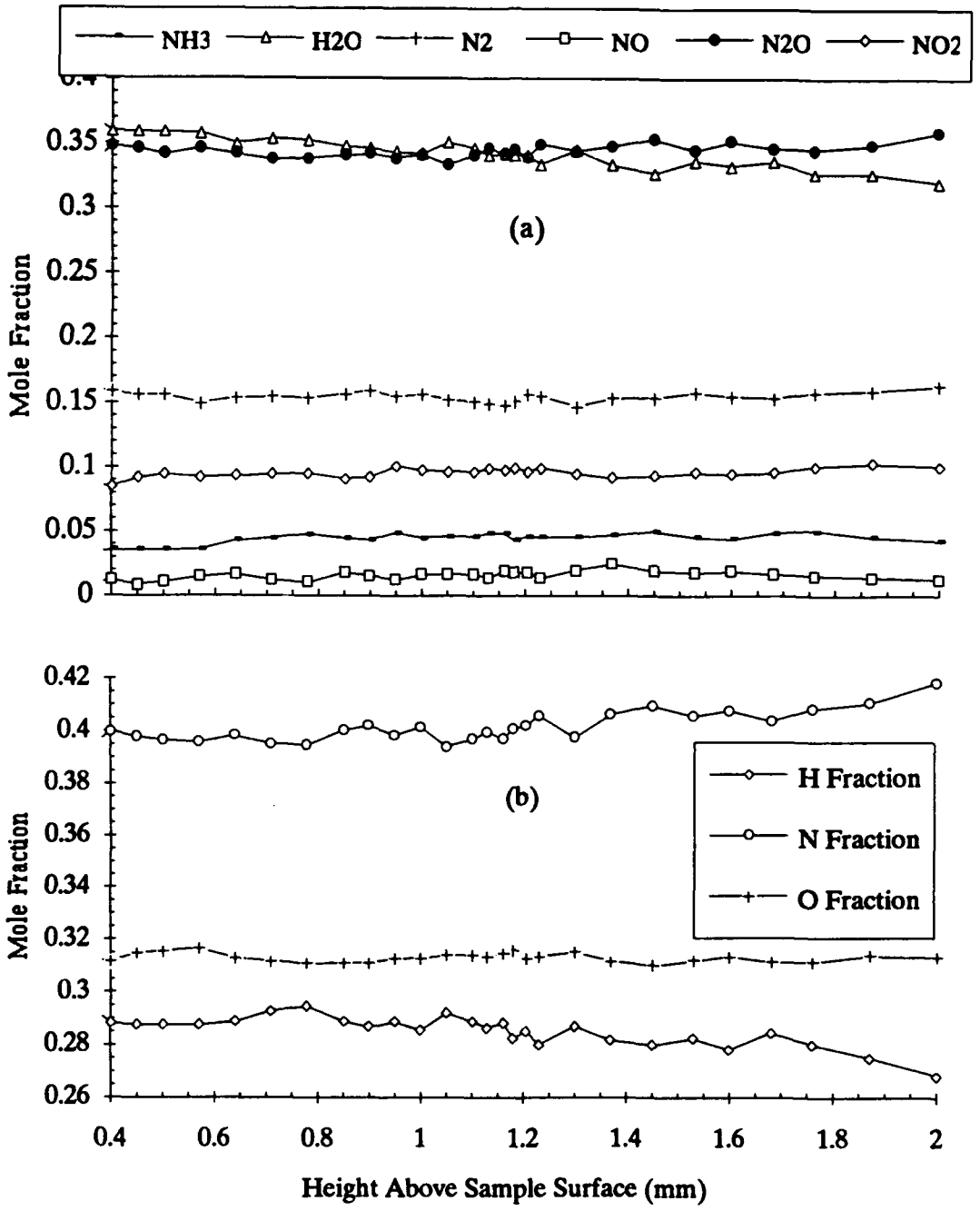

Figure 8. Spatial species profiles (a) and atom balances (b) for ADN at 1 atmosphere and a heat flux of 100 W/cm^2

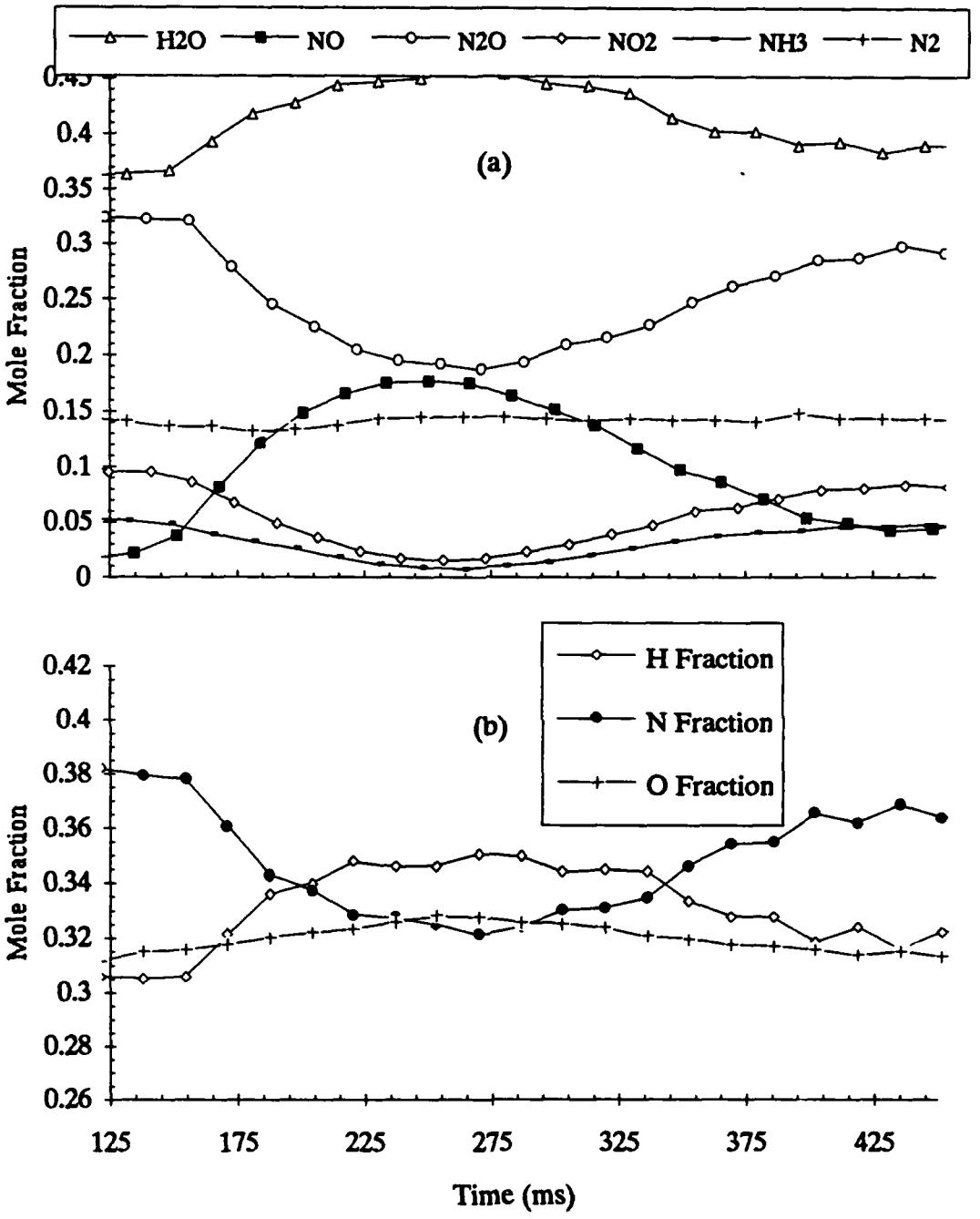

Figure 9. Species profiles (a) and atom balances (b) for ADN at 3 atmospheres in argon and a heat flux of 100 W/cm^2 with probe initially located 1.0 cm above the sample.

number of particles were initially evolved, but these particles were no longer evident after the flame was established. Figure 9b shows a very interesting pattern where the onset of a flame produces dramatic changes in the atom balances, bringing each balance much closer to the expected value of one-third. These results seem to indicate that as the flame develops, different mechanisms occur either in the near-surface gas phase or in the melt layer which preclude the formation of the particles. The atoms that make up the particles then become part of the species profiled in Figure 9a and restore the atom balance among the gas phase species. Brill et al. [3] state that NH_3 and HNO_3 would not recombine to form AN with a flame present but would react instead which is consistent with the results presented in Figure 9.

Figure 10 presents temporal species profiles and atom balances for another test at three atmospheres. In this test, the microprobe was initially located 0.6 cm above the sample surface and horizontally aligned with the side of the sample. The sample was allowed to burn away under laser heating with no positioner movement. A thin cylindrical flame sheet, which encircled the central jet of gases evolved from the sample, was observed at the location of the probe. In this test, no transient production of the flame was detected as a flame was immediately established near the probe tip location. The uniformity of the profiles in Figure 10 suggests that only post-flame gas species were measured throughout the test with no spatial changes in species mole fractions as the sample regressed. The species mole fractions closely match those at the center of the transient flame depicted in Figure 9. Figure 10b shows that the atom balances were quite consistent with that of ADN.

As stated previously, it appears that different mechanisms govern the energetic behavior of ADN depending on the test conditions. The decomposition of ionic salts containing ammonium, such as AN [4] and ammonium perchlorate (AP) [5], is usually initiated by proton transfer. For ADN, this implies the following initial reaction:

$$ADN \rightarrow NH_3 + HN(NO_2)_2 \qquad (1)$$

$HN(NO_2)_2$ may then decompose by loss of an NO_2 group [3] or by molecular rearrangement:

$$HN(NO_2)_2 \rightarrow NO_2 + HNNO_2 \qquad (2)$$

$$HN(NO_2)_2 \rightarrow HNO_3 + N_2O \qquad (3)$$

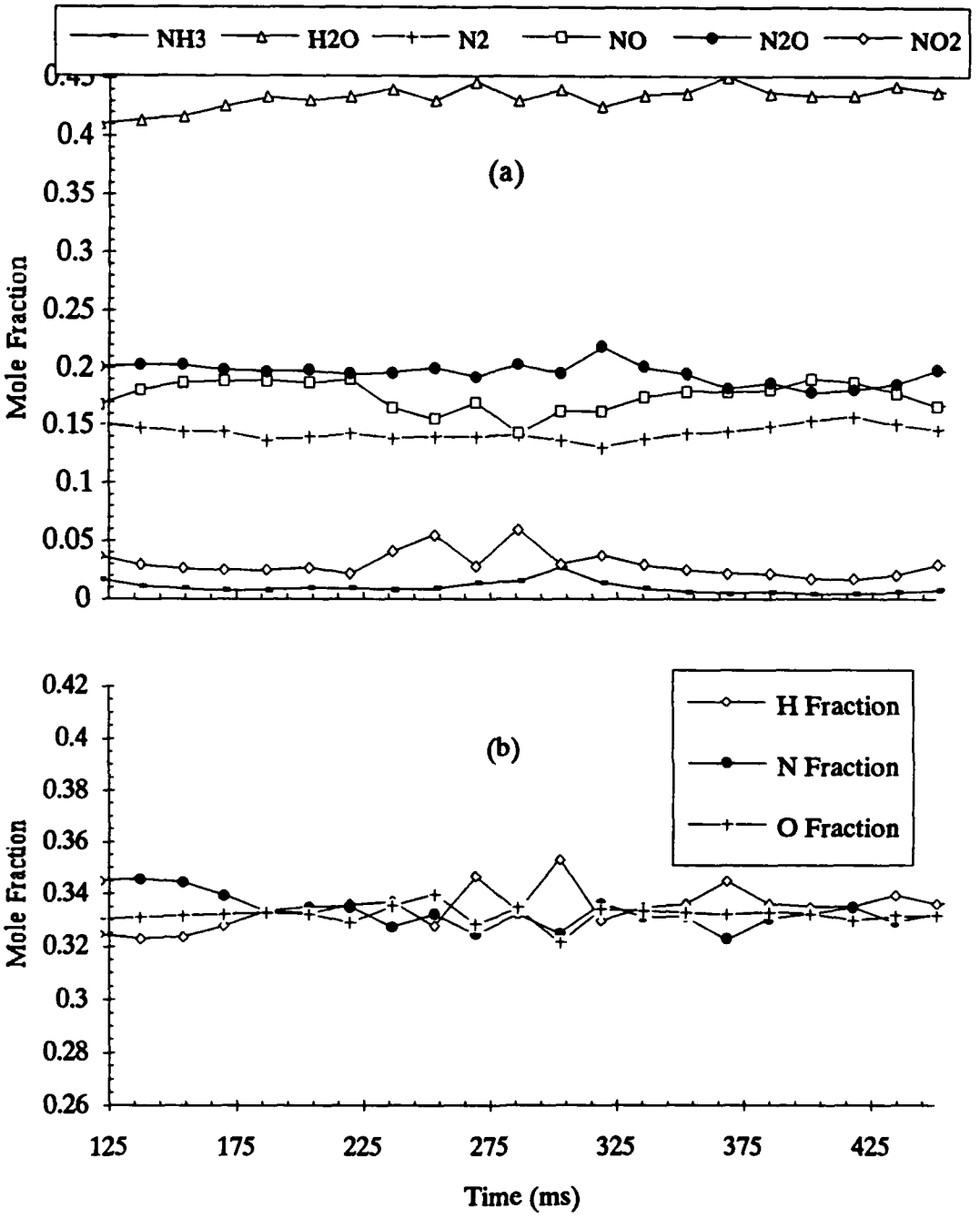

Figure 10. Species profiles and atom balances for ADN at 3 atmospheres in argon and a heat flux of 100 W/cm^2 with probe initially located 0.6 cm above the sample and aligned with the sample edge.

The $HNNO_2$ in Reaction 2 may then further decompose:

$$HNNO_2 \rightarrow N_2O + OH \qquad (4)$$

Decomposition Reactions 3 and 4 could produce the large fraction of N_2O evident in Figure 8. This decomposition sequence suggests that the large amounts of H_2O and N_2 must be produced by subsequent reaction of the products of the above reactions. In their proposed reaction scheme, Brill et al. listed the attack of OH on $HNNO_2$ and NH_3 as two reactions that would produce H_2O:

$$HNNO_2 + OH \rightarrow 2NO + H_2O \qquad (5)$$

$$NH_3 + OH \rightarrow H_2O + NH_2 \qquad (6)$$

Reaction of NO with the NH_2 radical could then generate both water and molecular nitrogen: [3,6,7]

$$NH_2 + NO \rightarrow N_2 + H_2O \qquad (7)$$

Reactions 1 through 7 are given only as possible pathways to the observed products of ADN pyrolysis and do not represent a complete mechanism. All these reactions are contained in the reaction scheme proposed by Brill et al. However, Brill et al. proposed that two branches may occur during rapid pyrolysis of ADN with one branch being Reaction 2 and the other being direct decomposition of ADN to NH_3, HNO_3, and N_2O which would result if Reactions 1 and 3 were combined.

The reactions mentioned above may be used to explain the trends in species mole fractions in the current study. At a pressure of one atmosphere where no flame exists, the NH_3 and HNO_3 produced in Reactions 1 and 3 may recombine to produce AN particles. However, when a flame is present, this recombination may not occur. These two species could then react to produce the flame products.[1] However, gaseous HNO_3 dissociates to OH and NO_2 as stated by Carleton et al. [8] and as listed in the NIST Chemical Kinetics Database: [9]

$$HNO_3 \rightarrow NO_2 + OH \qquad (8)$$

If Reaction 8 occurs then the NH_3/NO_2 reaction proposed by Brill et al. to be the major

source of heat release may occur. It should be noted that Brill et al. used the NH_3/NO_2 reaction in their reaction scheme for the initial decomposition of ADN, not for the luminous flame zone reaction. However, the trends in species profiles in Figure 9a and the consumption and production of species in Reaction 9 follow the same pattern, although the ratios of species produced do not match. Though the plot of mole fractions in Figure 9a does not indicate an increase in N_2, plotting the data in terms of actual concentrations showed that the amount of N_2 does increase by 3-4%.

The substantial production of NO and consumption of N_2O in Figure 9a are not predicted by the above set of reactions. A mechanism to explain these trends may be derived by first observing that about twice as much NO_2 is consumed in comparison to NH_3 consumption. The "extra" consumption of NO_2 could occur through its dissociation reaction, (10). Bedford and Thomas [6] stated that the dissociation reaction of NO_2 occurs at a rate comparable to the NH_3/NO_2 reaction:

$$2NO_2 \rightarrow 2NO + O_2 \qquad (10)$$

The consumption of N_2O could occur by radical reactions like those shown in Reactions 11 and 12.

$$N_2O + O \rightarrow 2NO \qquad (11)$$

$$N_2O + O \rightarrow N_2 + O_2 \qquad (12)$$

It should be reiterated that the above scheme is only a set of preliminary suggestions to explain the observed trends in species profiles. Kinetic modeling of these reactions and further experimentation will be undertaken to confirm the validity of the above reaction scheme.

RDX

Temperature profiles were not obtained for neat RDX because the high flame temperatures immediately burned out the fine-wire thermocouples. However, measurements were obtained for the surface temperature in tests below the critical heat flux where the flame zones establish. The surface temperature was 550 K for these no-ignition tests. Melius [10] calculated a surface temperature of 549K in his model of RDX combustion at one atmosphere. For tests where the

primary flame was established, a rapid rise in temperature was observed as the thermocouple left the melt layer, but the thermocouple was quickly burned out due to the intense flame.

Species profiles for deflagration of an RDX monopropellant under a heat flux of 200 W/cm^2 in argon at one atmosphere are displayed in Figure 11. These profiles are compilations from several different tests. At this heat flux, the primary flame zone occurs at about 200-300 μm above the sample surface and the secondary flame begins at a height of 500-600 μm. The slight separation of the two flame zones is believed to be due to the the laser-induced heating stretching out the spatial structure of the flame zones and preparation zones as mentioned by Parr and Hanson-Parr. [11] A violet-colored band about 200 μm thick was observed at the initiation of the secondary flame zone indicative of CN chemiluminescence. [11,12]. N_2 and CO were not included in these graphs due to some difficulties in obtaining the species profiles from the signal intensity at 28 amu throughout the gas-phase structure, especially in the regions around the primary and secondary flame zones where species mole fractions and temperatures change quickly. (This problem was subsequently resolved as discussed in the section of this report on the calibration of the mass spectrometer.) However, tests conducted to resolve the mole fractions of N_2 and CO in the secondary flame zone showed the mole fraction of both CO and N_2 to be about 0.30. Also, analysis of the data for several tests at different ionization potential settings showed that very little N_2 exists in the gas-phase before it is produced in the secondary flame. The mole fraction of CO was found to be about 0.03-0.05 near the surface and was assumed to be roughly constant leading up to the secondary flame. These data for N_2 and CO were used to approximate profiles for them throughout the gas-phase so that the mole fractions for the species depicted in Figure 11 could be calculated.

Figure 11 indicates that the primary flame zone reaction is principally due to the reaction of CH_2O and NO_2. The reaction produces a significant amount of NO and smaller amounts of H_2, CO_2, and H_2O. It is also believed that CO is produced to some extent in the primary flame. The reaction in the primary flame zone continues right up to the location of the initiation of the secondary flame as evidenced by the NO_2 profile. This structure corresponds well with results for a model by Melius [10] of the gas-phase flame chemistry of RDX that showed the luminous flame did not stand off from the primary flame but still maintained a spatial separation. Both HCN and N_2O remain relatively inert through the primary flame and are consumed in the secondary flame which starts at 500-600 μm above the surface. The primary reaction in the secondary flame is the reduction of NO by HCN which produces small

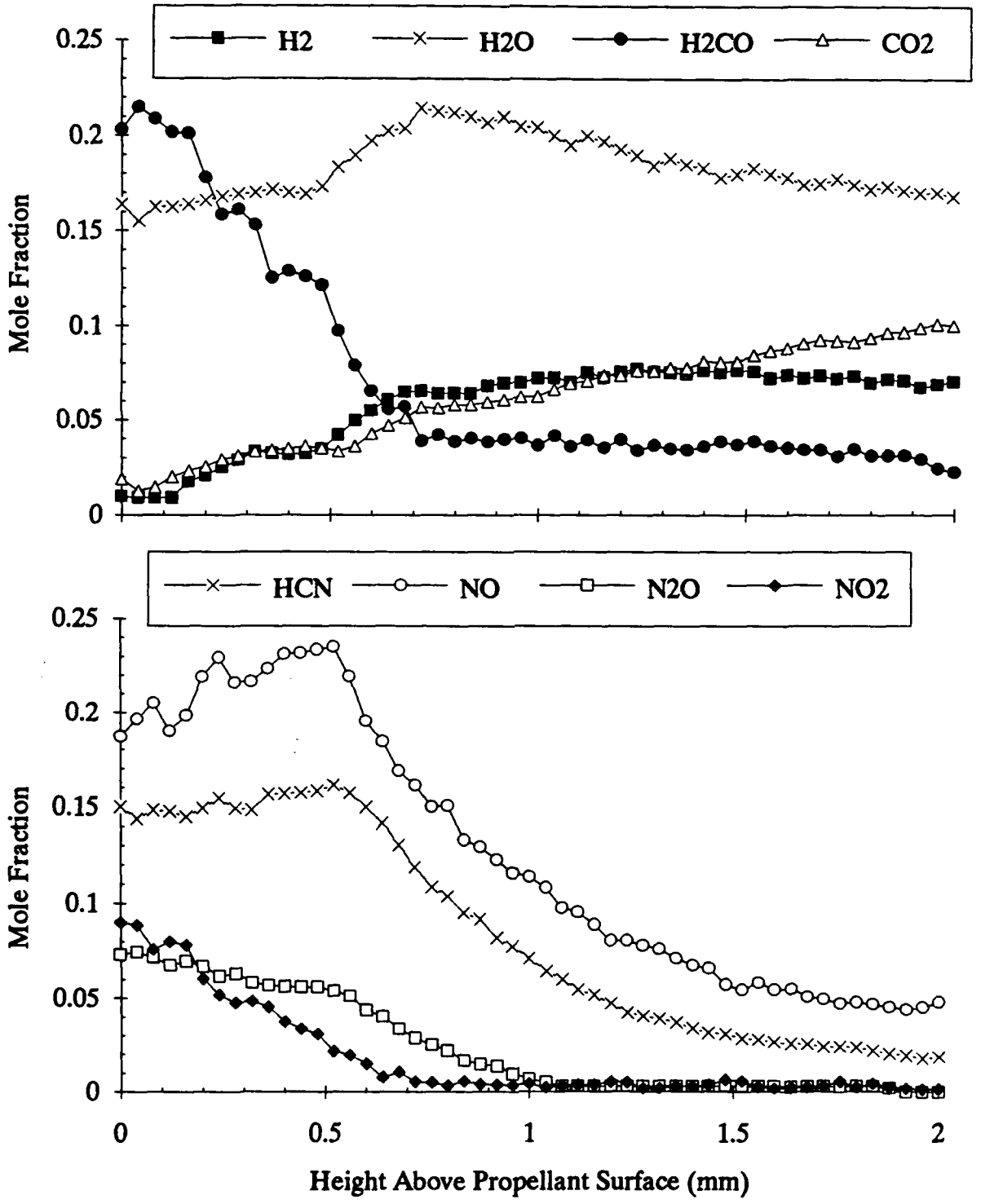

Figure 11. Species profiles for deflagration of RDX at a heat flux of 200 W/cm^2 in argon at 1 atmosphere

amounts of CO_2, H_2, H_2O, and substantial amounts of CO and N_2 (not shown in Figure 11). Korobeinichev et al. [13] also observed this reaction for the deflagration of RDX at a pressure of 0.5 atmosphere of argon. Their initial mole fractions of NO and HCN were both 0.22 whereas Figure 11 displays the same mole fraction of NO at the start of the secondary flame but only a mole fraction of 0.15 for HCN. However, the trends in product species profiles are quite similar to those of Korobeinichev et al. [13]

Several interesting physical phenomena were observed for the ignition and combustion of neat RDX. As the RDX monopropellant is heated, the solid melts and forms a melt layer on the surface as reported by numerous researchers. In the high-speed videos, the surface appeared to grow slightly at the onset of laser heating as the melt layer was established. If the level of incident heat flux was above a critical value of 43±5 W/cm^2, the primary flame was established, leading to subsequent quasi-steady burning of the monopropellant. However, if the heat flux level was below this critical value, no flame was established and the melt layer boiled vigorously with large bubbles evolved from the condensed phase. The thickness of the melt layer also became quite large as the heating time was increased. As the incident heat flux was increased far above the critical value, the surface boiling became more steady and well defined with the melt layer appearing to become considerably thinner as the heat flux was increased. These changes with heat flux could indicate that at low heat fluxes there is sufficient residence time for the liquefied RDX to decompose and/or vaporize in the thick melt layer with secondary reactions occuring between the evolved decomposition products, but as the heat flux is increased, the melt layer becomes thinner due to increased vaporization of the liquid and condensed phase chemical activity decreases due to decreased residence time.

XM-39 Composite Propellant

The species profiles for deflagration of XM-39 are given in Figure 12; the species profiles only go to within 750 μm of the surface due to residue buildup on the sample surface that disrupts the gas sampling. Reaction of CH_2O and NO_2 characteristic of the primary flame zone slowly takes place as the gases move away from the surface and rapid reactions characteristic of this zone occur relatively far from the surface from approximately 2.5 mm to 3 mm. Thus one effect of the binder is to lengthen the primary reaction zone relative to neat RDX. This observation is consistent with modeling studies of Melius. No secondary flame was observed at any level of incident heat flux in argon at one atmosphere.

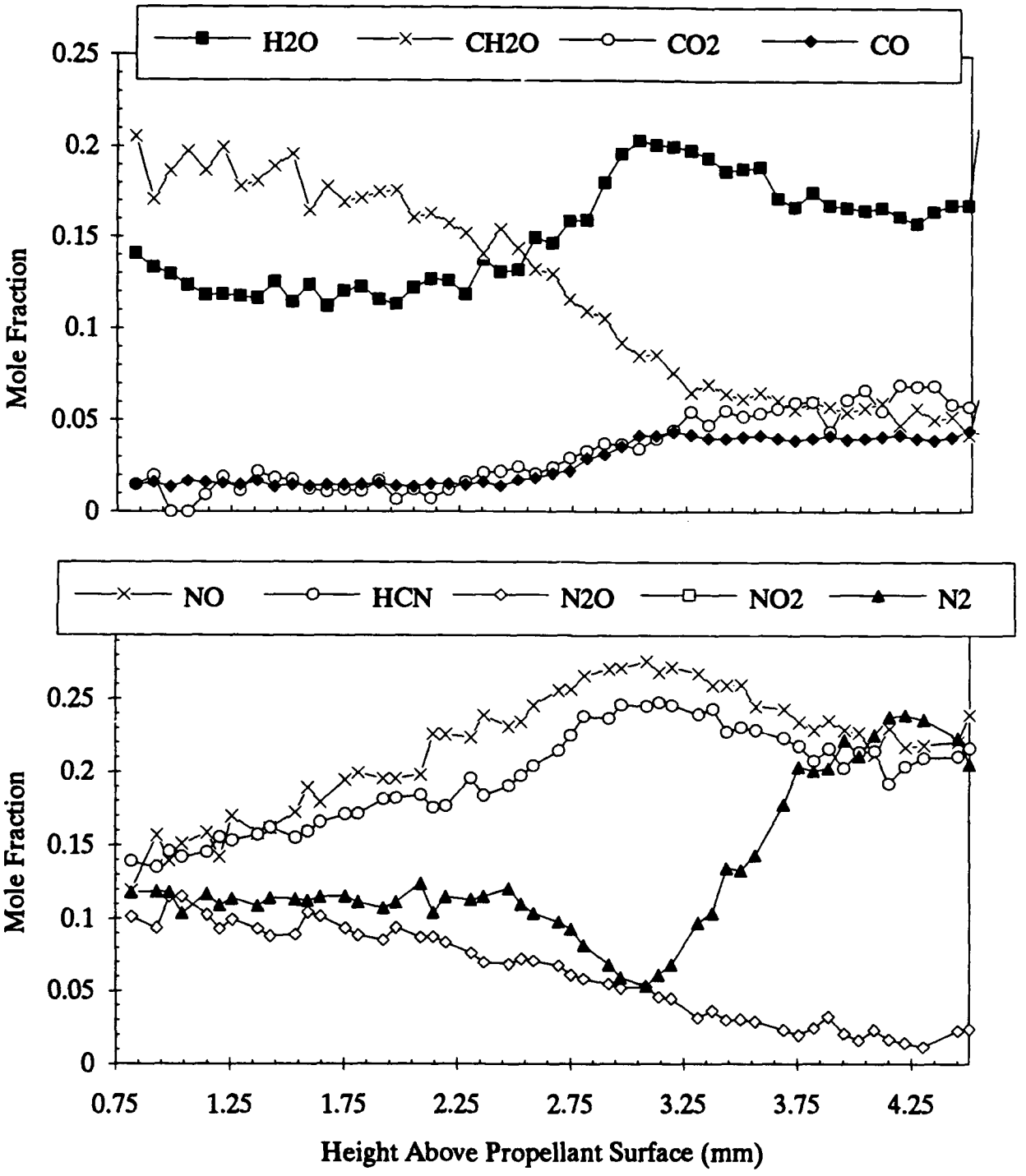

Figure 12. Species Profiles for deflagration of XM-39 at a heat flux of 200 W/cm^2 in argon at one atmosphere

CO was resolved with a high level of confidence at an ionization energy of 18 ev, but some difficulties were still encountered in resolving N_2. The atom balance shown earlier in Figure 6b indicates that the species mole fractions are consistent with those expected based upon the composition of the propellant. The mole fraction of H_2 was only approximately 0.005 throughout the measurement interval and was not included in Figure 12. Overall, the products of this primary flame are similar to those seen in RDX combustion with the CH_2O and NO_2 reacting to form NO, CO, and CO_2.

A temperature profile is displayed in Figure 13 for deflagration of XM-39 with an incident heat flux of only 100 W/cm^2. This profile shows the rapid primary flame reaction peaking beginning at about 3.25 mm. It is expected that this rapid temperature rise coincides with abrupt changes in species profiles displayed in Figure 12. The temperature profile exhibits interesting trends at the surface. Upon laser heating the surface temperature rapidly rose to 550 K as was also measured for RDX. Upon ignition and subsequent regression of the surface, the temperature rapidly rose to 650 K and then up to 700 K at 100 μm above the surface. This rapid rise in temperature near the surface is indicative of the decomposition zone where RDX and binder molecules decompose. After the decomposition zone, the temperature slowly rises corresponding to the slow reacton of NO_2 and CH_2O until rapid reaction occurs at 920 K with the temperature jumping to 1090 K and peaking at 1130 K at 4.5 mm.

Several tests were conducted at low heat fluxes of 35-50 W/cm^2 with the microprobe directly on the sample surface to investigate the pre-ignition evolution of gases leaving the surface. Upon laser heating, NO_2, NO, and HCN were evolved from the surface in a preignition puff. These species are simple molecules than can be derived directly from scission of the N-NO_2 bond and C-N bonds in the ring structure along with evolution of H and O atoms from bonds to C and N, respectively. The concerted dissociation scheme proposed by Zhao et al. [14] lists these molecules except for NO and also includes HONO. A small peak at 47 amu was observed, which may represent HONO, although this molecule is highly reactive and very difficult to detect. Small peaks were also observed at molecular weights of 52, representing C_2N_2, and at 73, which is believed to be an ionizer-induced fragment of N-nitroformimine (CH_2NNO_2) at 74 amu. As the sample was heated, the gases were evolved and then the melt layer began to grow and eventually immersed the probe tip. It is interesting to note that the peak at 73 grew as the melt layer began to immerse the probe, which suggests that there may be decomposition in the condensed phase of the RDX molecule producing the N-nitroformimine fragment of the ring structure as proposed by several researchers. However, this is only preliminary data that requires further investigation.

Additional tests were also performed to establish the effects of heat flux and pressure on the location and thickness of the primary reaction zone of XM-39. The NO_2 profiles from the different experiments are plotted in Figure 14 plotted as an indication of the primary reaction zone location and thickness; use of a single species permits a clearer comparison of the results. The results presented in Figure 14 indicate that increasing the heat flux at constant pressure and incresing the pressure at constant heat flux both caused the primary reaction zone to move closer to the surface. For neat RDX Parr and Hanson-Parr [15] observed that increasing the heat flux tended to blow the flame away from the sample surface and that increasing pressure caused the flame to move closed to the surface. Thus the presence of the binder appears to reverse the response of the material to changes in incident heat flux. Such information provides an interesting challenge for modellers of propellant combustion.

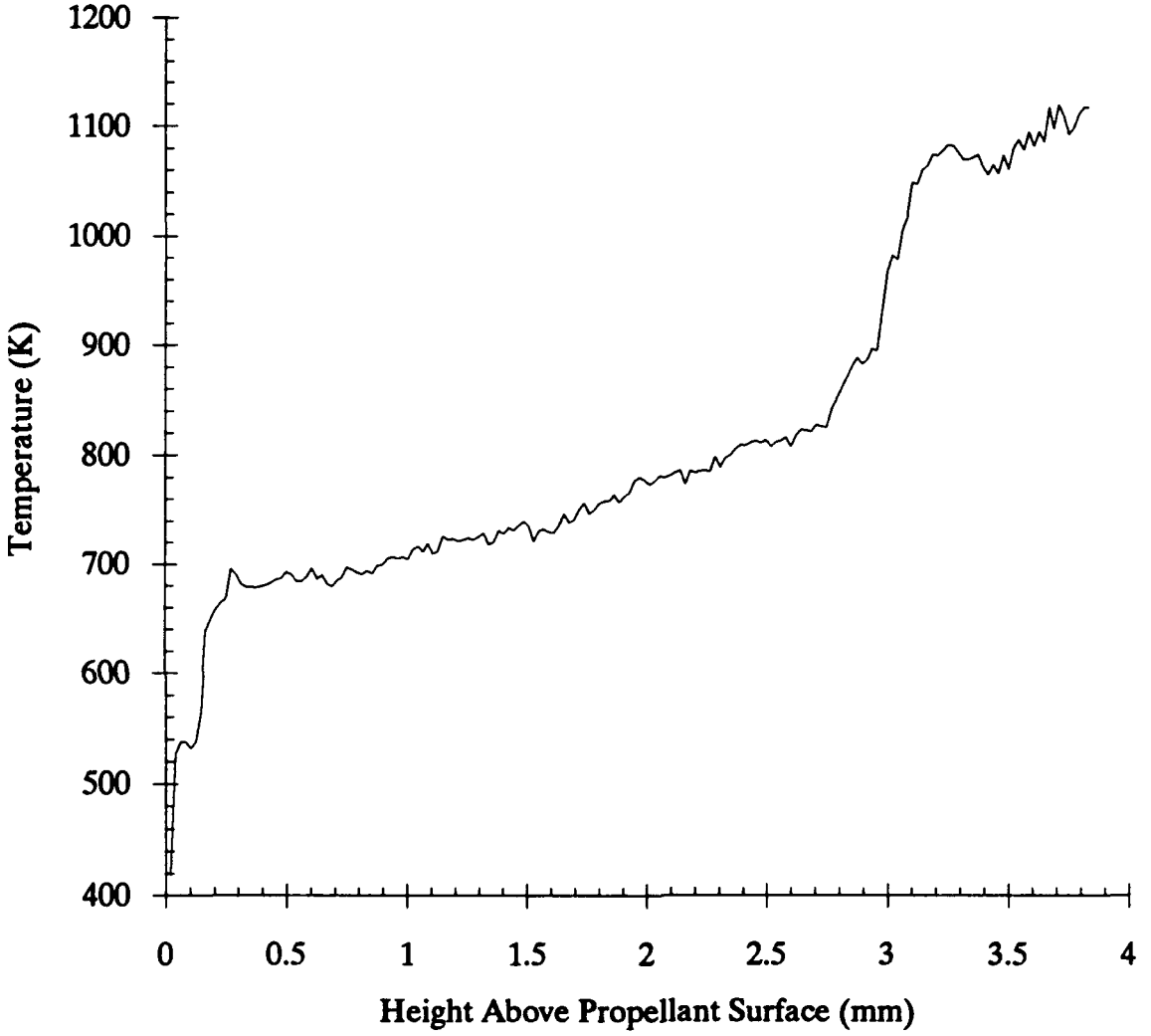

Figure 13. Temperature profile for deflagration of XM-39 at a heat flux of 100 W/cm^2 in argon at 1 atmosphere

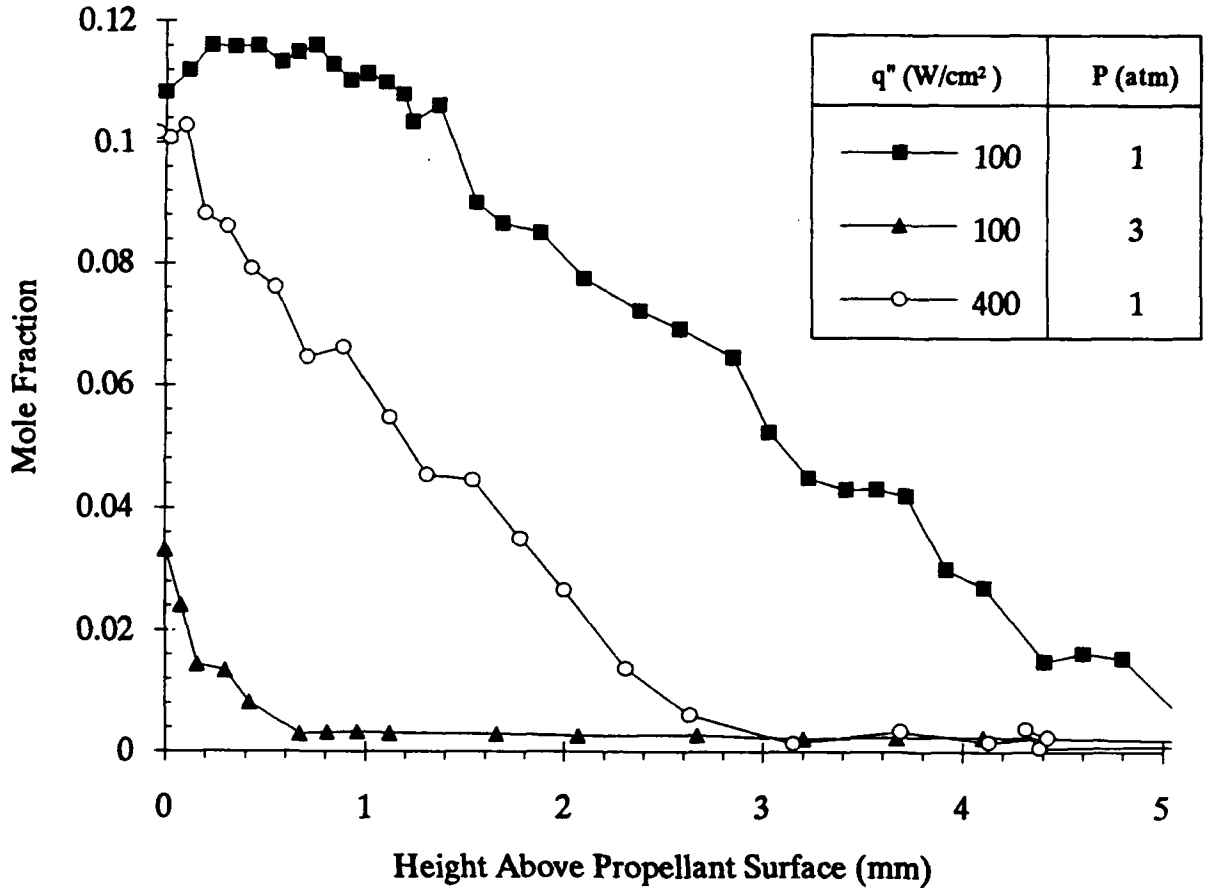

Figure 14. Comparison of NO_2 profiles for three different tests to establish the effects of pressure and heat flux on the thickness of the primary reaction zone in XM-39

REFERENCES

1. Isom, K. B., Caldwell, D. J., and Greene, F. T., "Pyrolysis of Nitramine Propellants II - Kinetic Experiments," 20th JANNAF Combustion Meeting, CPIA Publ. 383, Vol. II, Oct. 1983, pp. 17-23.

2. Fristrom, R. M., and Westenberg, A. A., Flame Structure, McGraw-Hill Book Co., 1965.

3. T. B. Brill, P. J. Brush, and D. G. Patil, "Thermal Decomposition of Energetic Materials 58. Chemistry of Ammonium Nitrate and Ammonium Dinitramide near the Burning Surface Temperature," Combustion and Flame, in press.

4. T. P. Russell and T. B. Brill, "Thermal Decomposition of Energetic Materials 31 - Fast Thermolysis of Ammonium Nitrate, Ethylenediammonium Dinitrate and Hydrazinium Nitrate and the Relationship to the Burning Rate," Combustion and Flame, Vol. 76, 1989, pp. 393-401.

5. N. E. Ermolin, O. P. Korobeinichev, A. G. Tereshchenko, and V. M. Fomin, "Measurement of the Concentration Profiles of Reacting Components and Temperature in an Ammonium Perchlorate Flame," Combustion, Explosion, and Shock Waves, Vol. 18, No. 1, Jan.-Feb. 1982, pp. 36-38.

6. G. Bedford and J. H. Thomas, "Reaction between Ammonia and Nitrogen Dioxide," Journal of the Chemical Society: Faraday Transactions I, 1972, pp. 2163-2170.

7. B. L. Fetherolf, P. M. Liiva, T. A. Litzinger, and K. K. Kuo, _Thermal and Chemical Structure of the Preparation and Reaction Zones for RDX and RDX Composite Propellants," 28th JANNAF Combustion Meeting, CPIA Publ. 573, Vol. II, Oct. 1991, pp. 379-386.

8. F. B. Carleton, N. Klein, K. Krallis, and F. J. Weinberg, "Laser Ignition of Liquid Propellants," Twenty-Third Symposium (International) on Combustion, The Combustion Institute, 1990, pp. 1323-1329.

9. W. G. Mallard, F. Westley, J. T. Herron, R. J. Cvetanovic, and R. F. Hampson, "NIST Chemical Kinetics Database, Version 3.0 -Data Coverage Through 1990," NIST Standard Reference Database 17, NIST Standard Reference Data, Gaithersburg, MD, 1991.

10. C. F. Melius, " The Gas-Phase Flame Chemistry of Nitramine Combustion," 25th Jannaf Combustion Meeting, CPIA Publ. 498, Vol. II, October, 1988.

11. T. Parr and D. Hanson-Parr, Species and Temperature Profiles in Ignition and Deflagration of HMX," Spring Meeting, Western States Section, The Combustion Institute, Provo, Utah, April, 1987.

12. M. C. Branch, M. E. Sadeqi, A. A. Alfarayedhi, and P. J. Van Tiggelen, " Measurements of the Structure of Laminar, Premixed Flames of $CH_4/NO_2/O_2$ and $CH_2O/NO_2/O_2$ Mixtures," Combustion and Flame, Vol. 83, pp. 228-239, 1991.

13. N. E. Ermolin, O. P. Korobeinichev, L. V. Kuibida, and V. M. Fomin, " Study of the Kinetics and Mechanism of Chemical Reactions in Hexogen Flames," Translated from Fizika Goreniya i Vzryva, Vol. 22, No. 5, pp. 54-64, Sept.-Oct. 1986, 0010-5082/86/2205-0544, Plenum Publishing Corp., 1987.

14. X. Zhao, E. J. Hintsa, Y. T. Lee, " Infrared Multiphoton Dissociation of RDX in a Molecular Beam," Journal of Chemical Physics, Vol. 88, No. 2, January, 1988.

15. T. Parr and D. Hanson-Parr, "Nitramine Flame Structure as a Function of Pressure," 26th JANNAF Combustion Meeting, CPIA Publ. 529, Vol. I, Oct. 1989, pp. 27-37.